AVO and Seismic Attributes Analysis of OTG Field, Deep Offshore Niger Delta

By

16010401009

Onimsi ThankGod.A

A Thesis

Submitted in Partial Fulfillment of the

Requirements for award of the Degree of

B.Sc. in Geophysics

Department of Geosciences

College of Basic and Applied Sciences

Mountain Top University

CERTIFICATION

I hereby certify that this research titled **AVO AND SEISMIC ATTRIBUTES ANALYSIS OF OTG FIELD, DEEP OFFSHORE NIGER DELTA**, prepared and submitted by ONIMSI THANKGOD. A with the matriculation number 16010401009 in partial fulfilment of the requirements of the degree of Bachelor of Science in Geophysics, is hereby accepted.

Mr. R.P AKINWALE _____

Supervisor *(Signature and Date)*

PROF. ELIJAH AYOLABI _____

Supervisor ` *(Signature and Date)*

DR. O.B BALOGUN _____

Head of Department *(Signature and Date)*

Accepted as partial fulfilment of the requirements for the degree of

Bachelor of Science in Geophysics,

Department of Geosciences.

DEDICATION

This project is dedicated to Almighty God for helping me reach a successful completion of this work.

ACKNOWLEDGEMENT

I would like to express my sincere gratitude to my supervisors Prof. Elijah Ayolabi and Mr. Rotimi Akinwale for their vital support, guidance and encouragement, without which this research would not have been completed.

I would also like to express my appreciation to the members of staff in the Department of Geosciences, Mountain Top University for their support during this completion of this project.

I would also like to specially thank the Visitor of the university, the General Overseer of the Mountain of Fire and Miracles Ministries, Dr. D.K. Olukoya for establishing this wonderful citadel of excellence giving me the privilege to attain a degree in this field and also improve in other ramifications of life.

I am extremely grateful to my parents Mr. and Mrs. Onimsi for their love, prayers and sacrifices for educating and preparing me for my future. I am very much grateful to my sponsors for their efforts and support to the completion of my academics.

Special thanks to my colleagues who also offered their assistance to the completion of this project, despite their busy schedule they were always available for me. Thank you.

TABLE OF CONTENTS

LIST OF FIGURES

LIST OF TABLES

Abstract

Amplitude variation with offset (AVO) analysis was carried out on OTG field, deep offshore Niger Delta for the purpose of predicting gas in the reservoirs. Exploration for oil and gas are being shifted to more complex and difficult terrain such as the deep offshore, quantitative studies such as AVO analysis are needed to reduce exploration risks associated with this environment. The dataset used for this study includes 3D seismic pre-stack migrated data with near and far offset gathers, full stack 3D seismic and composite well logs including compressional and shear sonics. Methods adopted involved the correlation of wells, generation of synthetic seismograms, surface attribute analysis, estimation of rock attributes, AVO modelling and classification of AVO anomaly type for subsequent prediction of fluids saturating the reservoir. Surface attributes analysis showed amplitude anomalies on the surface around the well tops indicating possible gas distribution. Cross plots of estimated rock attributes showed clusters that distinctively showed the distribution of fluid which are brine, oil and gas. Gradient versus intercept cross plot presented some of the plotted clusters as falling within the third quadrant and this was interpreted as indicative of the presence of gas in the reservoir. The AVO anomaly was classified as being of the class III type. Amplitude of reflection coefficients were observed to decrease with offset on seismic gather. The study concluded that though the reservoir was abundant in oil reserves, it contained significant amount of gas.

CHAPTER ONE

1.1 Introduction

Over the past years in the geosciences field, seismic amplitude-versus offset (AVO) analysis has been an effective geophysical tool in aiding the direct detection of gas-filled reservoirs from seismic records (Ohaegbuchu and Igboekwe 2016). AVO was founded on the findings of Koefoed (1955, 1962) that the variation in reflection coefficient of seismic waves with the incident angle, depends on the Poisson's ratio difference across an elastic boundary. He also propounded that critical observation of the orientation of the reflection coefficient versus angle of incidence curve could be a viable means of discriminating lithologies and their saturating fluid. Ostrander (1984) established a practical application of the amplitude variation with incident angle phenomenon. Further analyzing the reflection coefficients as a function of the angle of incidence for a simple three-layer, gas-sand model, he applied the Zoeppritz amplitude expressions from which he was able to discriminate sand and shale layers. This model was made of a sand layer encased in two shale layers (a similar geology to the geology of Niger Delta basin).

By using published values of Poisson's ratio for shale, brine saturated sands, and gas saturated sands, it was determined that there is a noteworthy enough variation in reflection coefficient with angle of incidence to differentiate between gas saturated sands and brine saturated sands. These theoretical observations were examined with real seismic data and established that AVO could be useful as a method of detecting gas sands (Coulombe *et al*., 1993). Generally, AVO is restricted by the assumptions and estimations intrinsic in surface seismic acquisition, processing, and interpretation. These factors include receiver arrays, near surface velocity variations, differences in geometrical spreading from near offset to far offset, dispersive phase distortion,

multiples interfering with primaries, wavelet phase, source directivity and array effects (pers. Comm. R. R. Stewart, 1990

1.2 Statement of Problem

In recent years, as the easy to find conventional hydrocarbon reserves in the earth's subsurface are

being exploited, the oil industries tend to search in more difficult terrains and much deeper waters to match the growing demand for fossil fuels. Therefore, exploration for oil and gas over time has advanced from being qualitative to quantitative. Quantitative studies of the subsurface generally and hydrocarbon fields in particular, require a lot of integrated data and analysis from geologists, geophysicists, petrophysicists, and reservoir engineers. Accurate characterization requires a combination of 3D seismic volume interpretations, amplitude analyses, rock physics and AVO (amplitude versus offset) analysis.

There are also exploration risks associated with the deep-water environment and this research is part of an effort to reduce those risks and to also identify exploration development opportunities away from the location within the study area.

1.3 Research Aim and Objectives

1.3.1 Aim

The aim of this study is to carry out AVO and Seismic Attribute analysis on OTG Field, in order to characterize gas in hydrocarbon reservoirs to reduce the exploration risk of oil and gas in Deep Offshore, Niger Delta.

1.3.2 Objectives

(i) Correlate the well logs in order to identify the reservoirs and characterize the fluid type.

(ii) Generate synthetic seismograms in order to map the horizons across the 3D seismic

(iii) Seismic interpretation and attributes analysis to indicate possible presence of hydrocarbon

(iv) Rock attributes estimation and evaluation for fluid distribution within the reservoir

(v) Perform AVO analysis on seismic data to identify the AVO classes and implication on the type of hydrocarbon saturating the reservoir.

1.4 Significance of Study

This research discusses the impact of observing common depth point gathers on Near, Mid and Far-offsets, to verify the credibility of the amplitude response in the prospect evaluation. It is also aimed at characterizing the fluid content or the lithology of a possible reservoir and reducing the exploration drilling risk in oil fields.

CHAPTER TWO

LITERATURE REVIEW

2.1 Review of Previous Works Done

AVO analysis of 3-D seismic data at G-field, Norway was carried out by Ogochukwu and Edmund (2014). Variations of amplitude depicted in survey vintages emphasized the activity of fluid contacts and variations in fluid compositions within the reservoir. AVO analysis was carried on the three wells. The analysis involved creating a synthetic model to deduct the amplitude responses observed at a particular reservoir horizon. Four types of fluid model substitution were created; pure brine, pure oil, pure gas and brine mix (70% Brine, 20% Gas and 10% Oil). Prominent amplitude changes which correspond primarily to the production effects was identified in the Tarbert reservoir.

AVO modelling was also carried out using pre-stack seismic and well-log data in the south-east Coastal Swamp of Niger Delta by Uko and Emudianughe (2014). The results of the work demonstrated that the seismic pre-stack and well-log data provided valuable information in modelling a reservoir and other important intervals in wells. Amplitude-Versus-Angle (AVA)/Amplitude-Versus-Offset (AVO) extracted from pre-stack seismic data identified gas sand of AVO Class 3 type. Sand-shale lithology is deduced, with sandstone volume decreasing with increasing depth, while shale volume increases with depth. Porosity and permeability showed decreasing trend with depth for both sandstone and shale units. Velocity, Gamma ray

(API), Poisson's ratio, Vp /Vs and density increase with increasing depth. Compressional-velocity Vp and shear-wave Vs are linearly related, and mudrock line equation is established for the study area: Vp =0.807Vs+1.600. Thus, the method was useful in the identification of prospective areas and also for feasibility studies during appraisal activity.

Ogagarue and Anine (2015) integrated rock physics, AVO modelling and analysis to identify reservoir fluid and lithology discrimination in a Niger Delta deep water block. This study was carried out to aid interpretation of seismic data and eventually reduce exploration risks associated with deep-water environments. This study involved the integration of rock physics and AVO technique in characterization and delineation of rock types and fluid effects, as well as delineate the seismic responses in the reservoir. The Castagna's mud rock line relationship was used to derive the in-situ shear wave log while the linearized Zoeppritz equations were used to model the seismic response at the reservoir top by the introduction of the various fluids using the Gassmann's equations. It was deducted from the outcome of the modelling that the sandstone reservoir exhibits a Class IV amplitude anomaly, and the Gassmann's simulated reservoir fluids could be clearly delineated within the reservoir except for the in-situ case using log data alone. Poisson's Ratio and Impedance relations were most effective in discriminating the gas sands. Results depicted amplitude anomalies away from the well bore, identifying possible prospective zones of hydrocarbon interests which was mainly gas.

A study including forward modeling from rock parameters measured from well logs and AVO analysis of events on pre-stack time migrated 3D seismic gathers was carried out by Ohaegbuchu and Igboekwe (2016) on Konga field, an onshore field in the Niger Delta. Forward modeling predicted specific AVO behaviour of anomalous reservoir sands in the field. AVO attributes (intercept and gradient) were derived from analysis of common depth point (CDP) gathers

obtained from a 3D pre-stack seismic survey. The attributes were cross-plotted to establish trends against which anomalous amplitude behaviour were identified. Reflections related to shales and brine sands exhibit a relatively small range of orientations creating a dominant ‘‘background trend’’ against which anomalous events related to hydrocarbon-saturated reservoirs show clear deviations. On the basis of cross plot analyses (reflectivity versus offset/angle and intercept versus gradient) and modeled acoustic impedance, Class 1 type AVO anomalies were observed and they were associated with non-hydrocarbon bearing clastic rocks that are most probably brine saturated in the field. These results however showed that drilling in this field in search of hydrocarbon reservoirs poses a risky venture.

Three AVO-based workflows were applied to marine seismic data acquired from offshore Norway by Mitchel and Rodrigo (2019) in order to emphasize the importance of AVO analysis on pre-stack gathers in aiding geoscientists in fluid identification and improved delineation of boundaries of hydrocarbon accumulation. The workflows were graphic visualization of amplitude versus offset curves, analysis of seismic volumes and cross-plots of intercept versus gradient, and interpretation of amplitude versus offset cube. In the case study, amplitude values increased significantly when the offset value increased, thus indicating the presence of gas.

2.2 Geology of the study area

The Niger delta province is situated in the south of Nigeria; it is bordered to the North by the Benin flank and to the south by the Atlantic Ocean. It extends from longitudes 3°E-9°E and latitudes 4°30′N - 5°20′N. The Niger Delta, located in the Gulf of Guinea of West Africa as illustrated in Figure 2.1, contains the Tertiary Niger Delta Petroleum System. The majority of the province lies within the borders of Nigeria where this study was carried out. Delineating lithology is not a difficulty in the Niger Delta because it is basically either shale or sand, and as such, it is suggested that the AVO analysis would be a more useful tool in the prediction of fluid type in the reservoirs.

2.2.1 Tectonics

The tectonic framework of the continental margin along the West Coast of equatorial Africa is controlled by Cretaceous fracture zones expressed as trenches and ridges in the deep Atlantic. The fracture zone ridges subdivide the margin into individual basins, and, in Nigeria, form the boundary faults of the Cretaceous Benue-Abakaliki trough, which cuts far into the West African shield. The trough represents a failed arm of a rift triple junction associated with the opening of the South Atlantic. In the region of the Niger Delta, rifting diminished altogether in the Late Cretaceous. After rifting ceased, gravity tectonism became the primary deformational process. Shale mobility induced internal deformation and occurred in response to two processes (Kulke, 1995). First, shale diapirs formed from loading of poorly compacted, over-pressured, prodelta

and delta-slope clays (Akata Fm.) by the higher density delta-front sands (Agbada Fm.). Second, slope instability occurred due to a lack of lateral, basin-ward, support for the under-compacted delta-slope clays (Akata Fm.). For any given depobelts, gravity tectonics were completed before deposition of the Benin Formation and are expressed in complex structures, including shale diapirs, roll-over anticlines, collapsed growth fault crests, back-to-back features, and steeply dipping, closely spaced flank faults (Evamy *et al*., 1978; Xiao and Suppe, 1992). These faults mostly offset different parts of the Agbada Formation and flatten into detachment planes near the top of the Akata Formation.

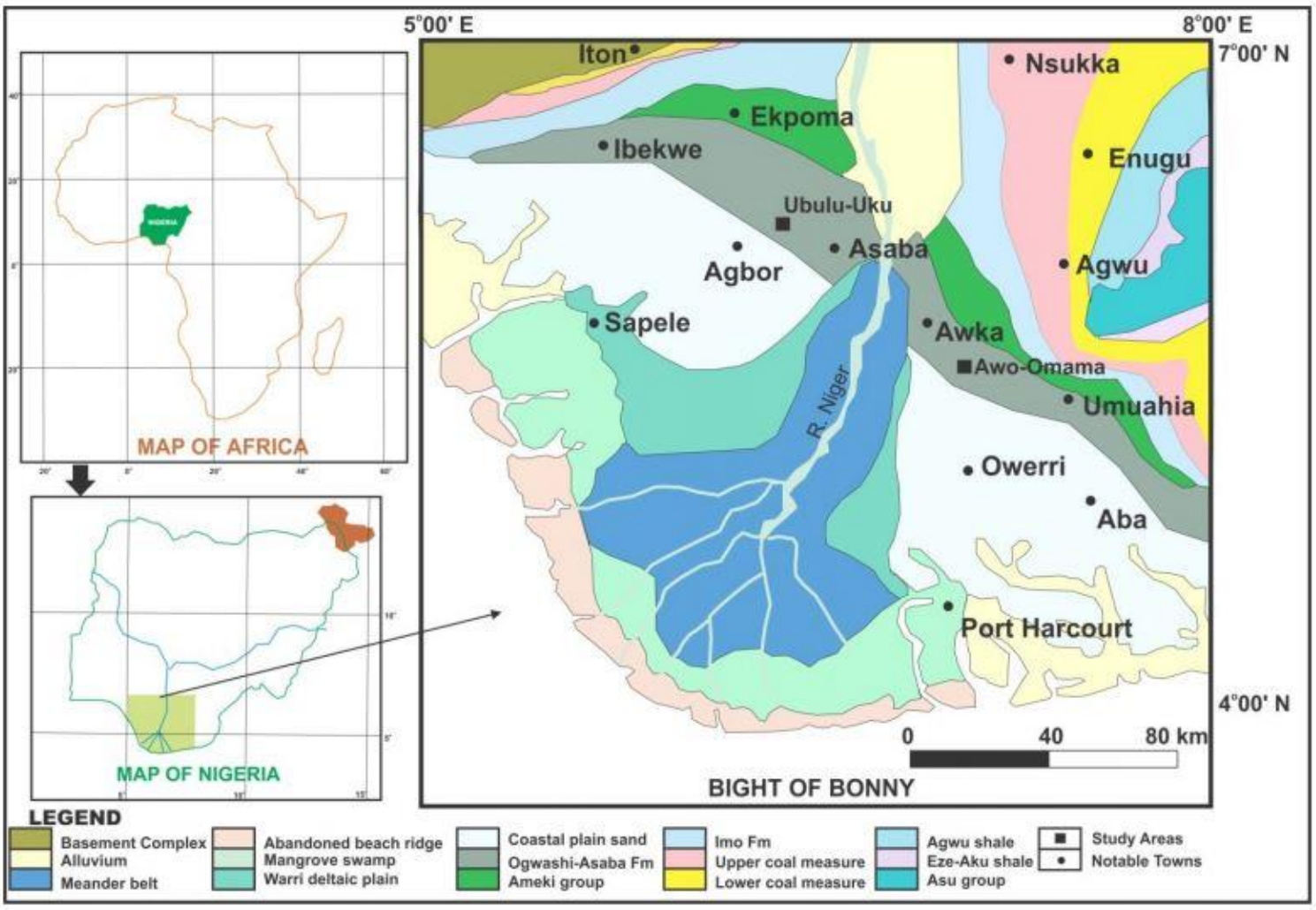

Figure 2.1 Geology Map of Niger Delta (after Nwajide C.S., 2013)

2.2.2 Lithology

Akata Formation

The Akata Formation (figure 2.2) is the major time transgressive lithological unit of the Niger Delta. It is mainly marine mud facies with turbiditic sands and continental slope channel fills. The formation underlies the whole of the Niger Delta complex south of the Imo Shale outcrop area and is taken as the up-dip equivalent of the Akata lithofacies (Whiteman, 1982). At present the Akata facies is being deposited on the continental shelf and slope and perhaps on the lower part of the prodelta slope. The Akata Formation consists of dark gray uniform shales, especially in its upper part. It tends to be sandy in the upper parts from where it grades into the Agbada Formation. The top of the formation is not clearly defined. It is taken arbitrarily as the deepest development of deltaic sandstones assignable to the Agbada Formation. Formation thickness ranges from 2,000 ft. to 20,000 ft. From the abundant planktonic foraminifera, the formation is inferred to have been deposited in a relatively deep open marine shelf setting.

Agbada Formation

The Agbada Formation (figure 2.2) underlies the Benin Formation and it consists of intercalations of shale and sandstone lithologies. The Agbada Formation is the main reservoir rock of the basin while its shale layers as well as those of the underlying formation serve as the source rocks. This unit constitutes the middle part of the tripartite Niger Delta stratigraphic succession. The formation is strongly diachronous, ranging in age from Eocene to present day.

The mangrove swamp to coastal barriers and fluviomarine zones of the present-day delta constitute the surface exposure of Recent age.

Benin Formation

According to Short and Stable (1967) this unit consists predominantly of continental fluvial sands that underlie an extensive area of southern Nigeria typified by the sands around Benin City where it is estimated to be 3050 m thick. The unit is generally friable and consists of white, fine to coarse and pebbly, poorly sorted sands. Lignite occurs as thin streaks or as finely dispersed fragments. Within the formation are thin grayish brown shale bands containing plant fragments. The Benin Formation is reconstructed as the upper and lower flood (delta) plain setting. Also involved are deltaic, estuarine, lagoonal, and fluviolacustrine sub-environments. Although some marine shale breaks have been identified within the formation, the bulk of the belt facies (Allen, 1965a; Dessauvagie, 1972). The shale breaks probably are the source of the fossils on which Reyment (1965) based the observation that the formation is "partly marine, partly deltaic, partly estuarine, partly lagoonal, and fluviolacustrine in origin." The age is Eocene to Recent (Short and Stauble, 1967; Whiteman, 1982.). In the southeastern parts of the offshore Niger Delta, the Benin Formation extends from the ocean bottom with a thickness of about 914 m. It retains its characteristics as a deposit consisting of fine to coarse grained, pebbly, poorly sorted, feldspathic and hematitic quartz sand, interbedded with shales, and occasional lignite streaks. The formation here is primarily nonmarine to paralic onshore, but becomes neritic in the offshore. (Opara, 1981). Its basal shale beds, with some sands, have been dated Pliocene to Recent, and designated informally as a member of the Benin Formation. The formation is hydrocarbon bearing in some

of the Mobil fields, contrary to the situation elsewhere where it is solely water bearing. In several parts of the subsurface Niger Delta, within the Agbada and Benin Formations, deep and relatively a really extensive erosional canyons are found filled with clays and subordinate sands. They occur in both the eastern and western re-entrants of the delta, but are more common in the eastern side. Their location has been attributed to ocean current action at the re-entrants of the Nigerian coastline. The canyons are said to represent erosional processes during relative sea level falls, followed by canyon filling during the subsequent relative sea level rises. At those low stands of the sea, the Niger Delta built pronouncedly seaward and in fact became a shelf edge delta with sediment debouching as turbidity flows that nourished deep sea fans.

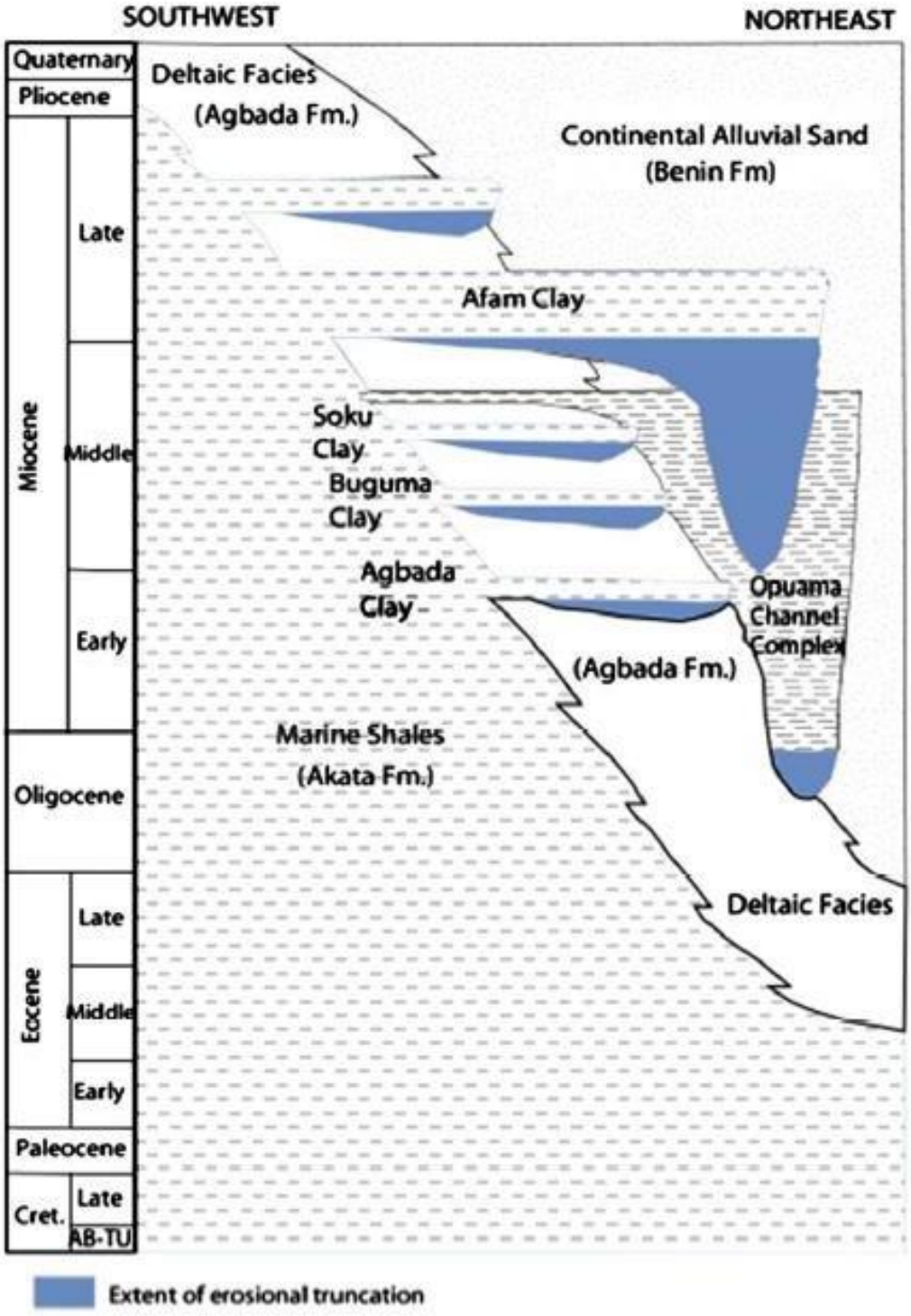

Figure 2.2 Stratigraphy column of the Niger Delta basin (after Ozumba *et al.* 2013)

2.2.3 Depobelts

Deposition of the three formations occurred in each of the five off-lapping siliciclastic sedimentation cycles that comprise the Niger Delta. These cycles (depobelts) are 30-60 kilometers wide, prograde southwestward 250 kilometers over oceanic crust into the Gulf of Guinea (Stacher, 1995), and are defined by synsedimentary faulting that occurred in response to variable rates of subsidence3 and sediment supply (Doust and Omatsola, 1990). The interplay of subsidence and supply rates resulted in deposition of discrete depobelts-- when further crustal subsidence of the basin could no longer be accommodated, the focus of sediment deposition shifted seaward, forming a new depobelt (Doust and Omatsola, 1990). Each depobelt is a separate unit that corresponds to a break in regional dip of the delta and is bounded landward by growth faults and seaward by large counter-regional faults or the growth fault of the next seaward belt (Evamy *et al*., 1978; Doust and Omatsola, 1990). Five major depobelts are generally recognized, each with its own sedimentation, deformation, and petroleum history. Doust and Omatsola (1990) describe three depobelt provinces based on structure. The northern delta province, which overlies relatively shallow basement, has the oldest growth faults that are generally rotational, evenly spaced, and increase their steepness seaward. The central delta province has depobelts with well-defined structures such as successively deeper rollover crests that shift seaward for any given growth fault. The distal delta province is the most structurally complex due to internal gravity tectonics on the modern continental slope (Figure 2.3).

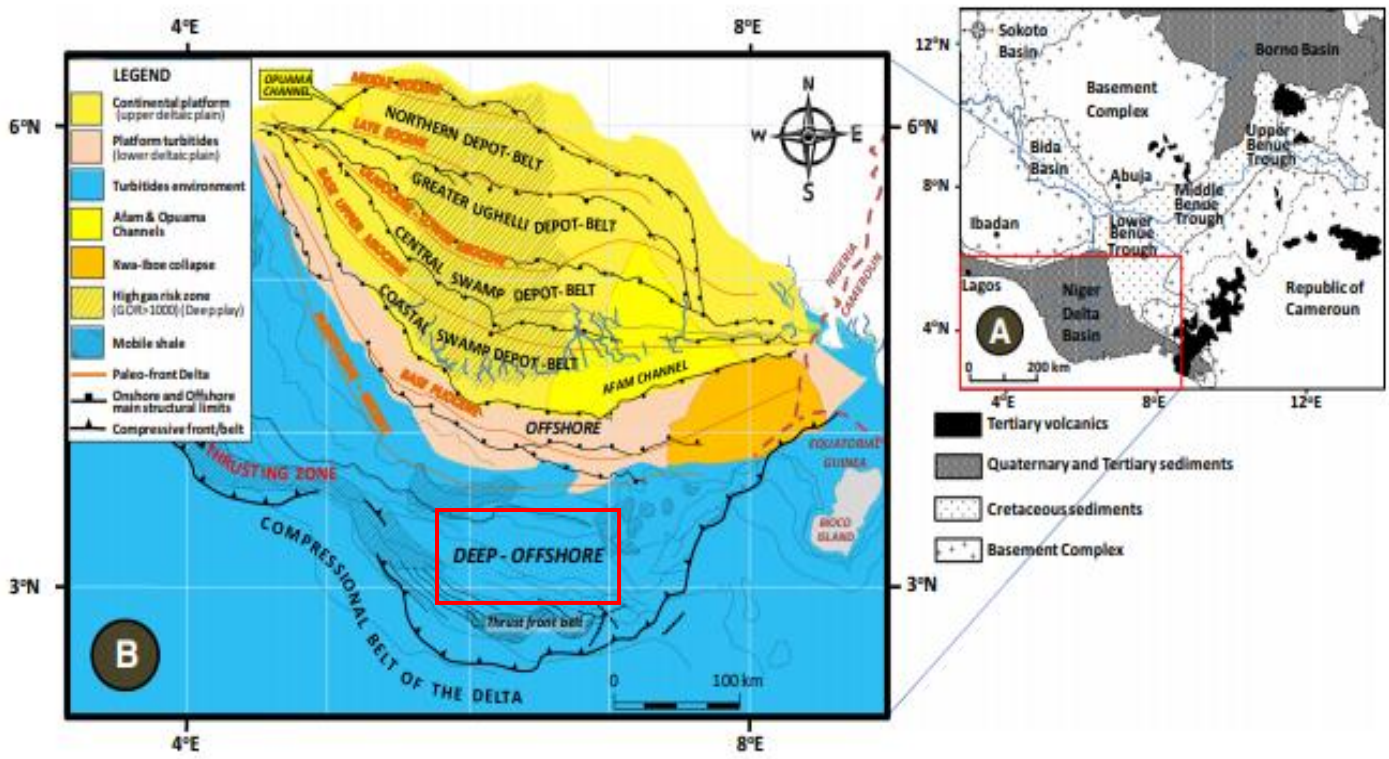

Figure 2.3 Geologic map of Nigeria showing the location of the Niger Delta Basin (a) (after Ebong *et al*. 2017) and sectional map of the Niger Delta depobelts and structural limits (b) (from Ebong et al. 2017) Study area is highlighted in red box.

2.3 Basic Theory

2.2.1 Rock Physics

There are a large number of rock physics models and relations that provide tools for data QC, characterization and generation of model scenarios. Commonly used are the models are categorized below as;

1. Gassmann's equation
2. Empirical models: Vp – Vs Relation
3. Theoretical bound (Hashin–Shtrikman)
4. Contact models

Gassmann's relations

One of the most important problems in the rock physics analysis of logs, cores, and seismic data is using seismic velocities in rocks saturated with one fluid to predict those of rocks saturated with a second fluid, or equivalently, predicting saturated-rock velocities from dry-rock velocities, and vice versa. This is the fluid substitution problem. Generally, when a rock is loaded under an increment of compression, such as from a passing seismic wave, an increment of pore-pressure change is induced, which resists the compression and therefore stiffens the rock. The low-frequency Gassmann–Biot (Gassmann, 1951; Biot, 1956) theory predicts the resulting increase in effective bulk modulus, K(sat), of the saturated rock using the following equation below:

$$\frac{K_{sat}}{K_0 - K_{sat}} = \frac{K_{dry}}{K_0 - K_{dry}} + \frac{K_{fl}}{\emptyset(K_0 - K_{fl})}, \mu_{sat} = \mu_{dry} \quad (1)$$

where K(dry) is the effective bulk modulus of dry rock, K(sat) is the effective bulk modulus of the rock with pore fluid, K_0 is the bulk modulus of mineral material making up rock, K(fl) is the effective bulk modulus of pore fluid, f is the porosity, μ(dry) is the effective shear modulus of dry rock, and μ(sat) is the effective shear modulus of rock with pore fluid.

Gassmann's equation assumes a homogeneous mineral modulus and statistical isotropy of the pore space but is free of assumptions about the pore geometry. Most importantly, it is valid only at sufficiently low frequencies such that the induced pore pressures are equilibrated throughout the pore space (i.e., there is sufficient time for the pore fluid to flow and eliminate wave-induced pore-pressure gradients). This limitation to low frequencies explains why Gassmann's relation works best for very low-frequency in-situ seismic data (<100 Hz) and may perform less well as frequencies increase toward sonic logging (about 10^4 Hz) and laboratory ultrasonic measurements (about 10^6 Hz).

P-wave Velocity – S wave Velocity relations

V_p–V_s relations are key to the determination of lithology from seismic or sonic log data as well as for direct seismic identification of pore fluids using, for example, AVO analysis. Castagna *et al.* (1993) give an excellent review of the subject. There is a wide and sometimes confusing variety of published V_p–V_s relations and V_s prediction techniques, which at first appear to be quite distinct.

The fact remains that the most reliable and most often used V_p–V_s relations are empirical fits to laboratory or log data, or both. The most useful role of theoretical methods is extending these empirical relations to different pore fluids or measurement frequencies, which accounts for the two steps listed above. A summary of a few of the popular V_p–V_s relations compared with laboratory and log data sets and illustrate some of the variations that can result from lithology, pore fluids, and measurement frequency was discussed.

Sandstones and shales

Figures 2.4 and 2.5 show laboratory V_p–V_s data for water-saturated sandstones and shales from Castagna *et al*. (1985, 1993) and Thomsen (1986), as compiled by Castagna *et al*. (1993). Superimposed, for comparison, are a least-squares linear fit to these data offered by Castagna *et al.* (1993)

$V_s = 0.794V_p - 0.787$ (km/s)

This relation by Han (1986) and Castagna *et al*. (1985) give the best overall fit to the sandstones. The mudrock line predicts systematically lower Vs because it is best suited to the most shaley samples, as shown in Figure 2.4. Castagna *et al.* (1993) suggest that if the lithology is well known, one can fine tune these relations to slightly lower V_s/V_p for high shale content and higher V_s/V_p in cleaner sands. When the lithology is not well constrained, (Han and the Castagna *et al*.) lines give a reasonable average.

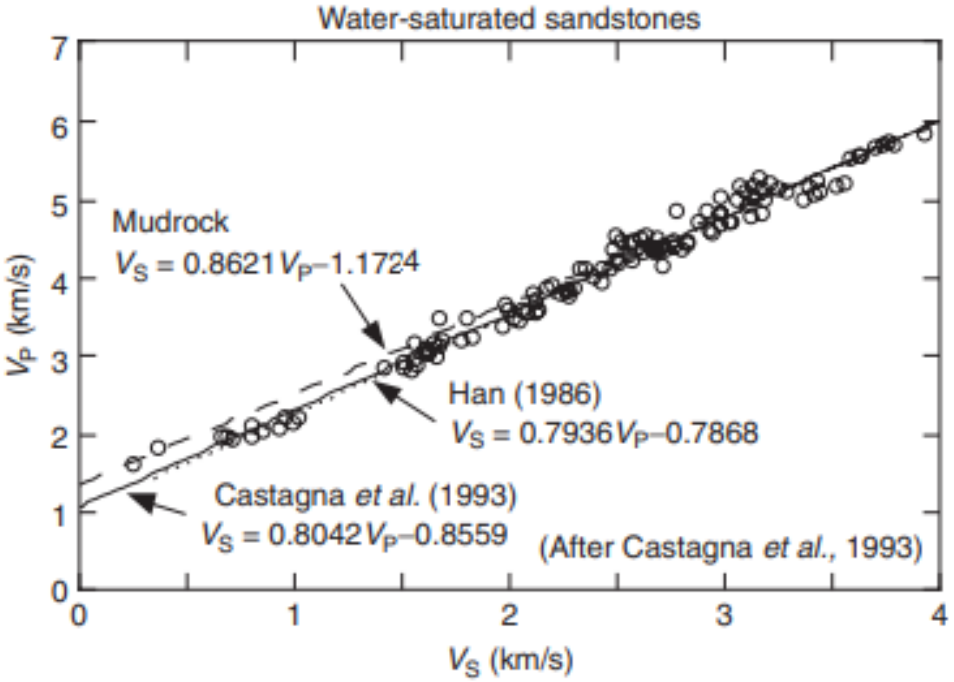

Figure 2.4 Laboratory Vp-Vs data for water-saturated sandstones (Mavko *et al*., (2009)

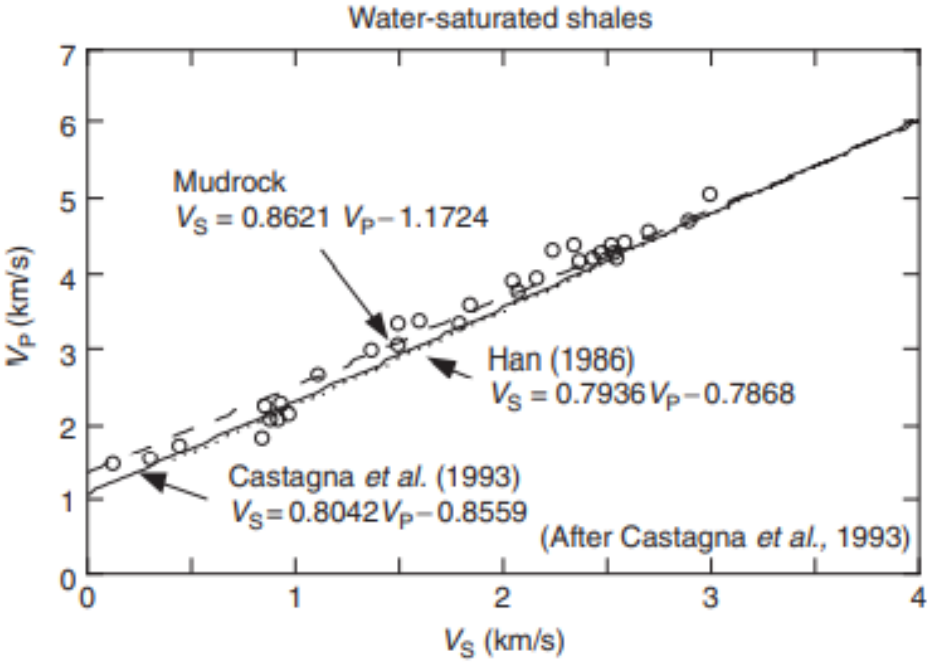

Figure 2.5 Laboratory Vp-Vs data for water-saturated sandstones (Mavko et al 2009)

2.3.2 Theory of AVO

Amplitude Variation with offset (AVO) method evaluates disparities in seismic reflection amplitude with differences in distance between receivers and shot points. The AVO analysis permits geophysicists to better evaluates reservoir rock properties, including porosity, density, lithology and fluid content. In the early 90s, Knott and Zoeppritz came up with the theoretical work essential for theory of AVO (Knott, 1899; Zoeppritz, 1919), given that the P-wave and S-wave velocities alongside with the densities of the two-bounding media. Plane-wave reflection amplitudes expressions are a function of incident angle were developed. Subsequently the Zoeppritz's equation was modified by Bortfeld (1961), making it less difficult to comprehend how reflection amplitudes is dependent on incident angle and physical parameters. The relation of AVO to change in Poisson's ratio across a boundary was outlined by Koefoed (1955). The results were on the basis of exact Zoeppritz equation. Hence Koefoed's deductions are the basis of today's AVO interpretation. Inspired by Koefoed's work, Shuey (1985) made a quantum leap in the work in relation to lithology prediction from AVO. Ostrander (1982) defined the advantages of AVO interpretation with field data, fast-tracking the discovery of amplitude interpretation. Subsequently Allen and Peddy in 1993 collected seismic data, well information, and interpretation from the Gulf Coast of Texas and published a practical approach at AVO that recorded not only successes but also the interpretational failures learned from dry holes. Attributes (seismic amplitude) at layer boundaries are a function of the variations of the physical attributes immediately below and above the interfaces which has led to AVO analysis becoming a common tool in detection of hydrocarbon, lithology identification, and fluid parameter analysis. In recent years, theories and techniques in data acquisition, processing, and

interpretation of seismic data have been modified extensively. Generally, AVO analysis is becoming progressively lucrative.

2.4 Principles of AVO

Seismic waves propagated via the subsurface and comes in contact with lithology interfaces with contrasting velocities and densities, the energy of the incident wave is partitioned at each interface as illustrated in figure 2.6. A fraction of the incident energy associated with a compressional source is transformed to a shear wave concretely; then both the compressional and shear wave energy are reflected and transmitted partially via the boundaries of these layers. The angle of incidence influences the fraction of the incident energy that is reflected. Reflection amplitudes evaluation as a function of incidence angle can sometimes be used to delineate changes in elastic properties of reservoir rocks, such as the change in Poisson's ratio. A change in the ratio of velocity of primary wave to shear wave velocity which could be as a result of change in fluid saturation within the reservoir rocks. The wave equations for plane elastic waves in an isotropic media can be derived and resolved starting with the equations of motion and Hooke's law. The continuity equations for the vertical and tangential components of stress and strain at a layer interface, plane wave solutions and Snell's law that relates propagation angles to wave velocities. Hence the derivation of the expression for computing the waves' amplitudes are obtained.

Approximations of the Zoeppritz Equations

The exact plane wave amplitudes of a reflected P wave as a function of angle, can be derived in respect to Zoeppritz equations but how these amplitudes relate to the various physical parameters is not intuitively comprehended. Subsequently several approximations to the Zoeppritz equations

have been made the first being Bortfeld's (1961). His approximation to the Zoeppritz equation for PP reflection amplitude expressed as:

$$R(\theta) = \frac{1}{2}\ln\left(\frac{\alpha_2\rho_2\cos\theta_2}{\alpha_1\rho_1\cos\theta_1}\right) + \left[2 + \frac{\ln\frac{\rho_2}{\rho_1}}{\ln\frac{\alpha_2}{\alpha_1} - \ln\frac{\alpha_2\beta_1}{\alpha_1\beta_2}}\right]\frac{\beta_1^2 - \beta_2^2}{\alpha_1^2}\sin^2\theta. \qquad (2.1)$$

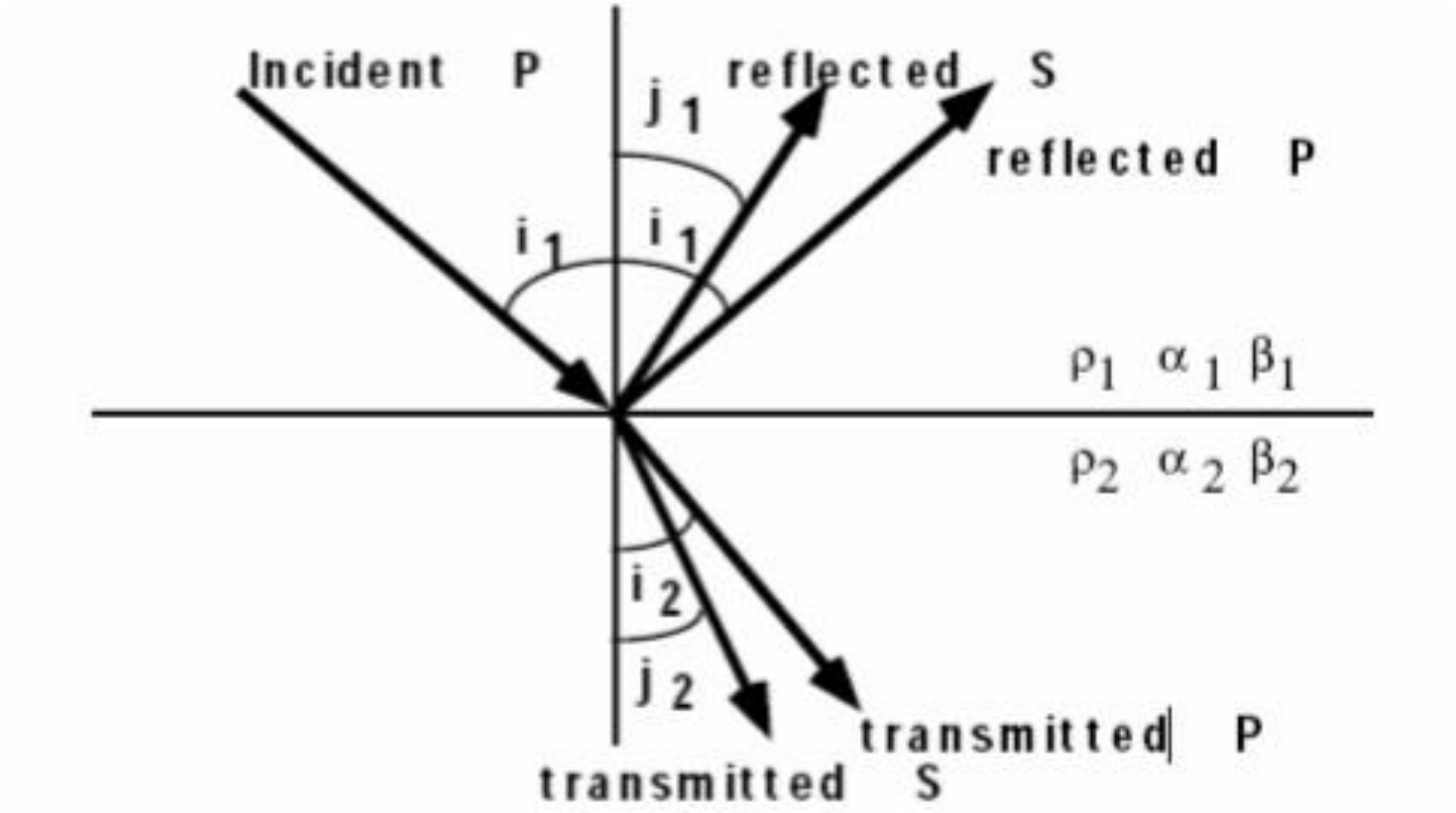

Figure 2.6 Wave propagation of incidence of compressible wave at solid-solid interface.

A significant feature of Bortfeld's equations is, they provide an insight into the amplitude variation with offset as a function of rock properties. The first term in Bortfeld's PP equation is fluid-fluid reflection coefficient. The second term has been called the rigidity term because of its dependence on the S-wave velocity, and thus on the shear rigidity modulus. However, equation (2.1) does not explicitly indicate angle- or offset- dependence of reflection amplitudes; therefore, its practical implementation for AVO analysis has not been considered.

Subsequently Richards and Frasier (1976) modified the Bortfeld approximation followed by Aki and Richards (1980). The Aki, Richards and Frasier approximation are better because it is depicted as three terms, the first involving P-wave velocity, the second involving density, and the third associated with S-wave velocity. Their formula is expressed thus:

$$R(\theta) = a\frac{\Delta\alpha}{\alpha} + b\frac{\Delta\rho}{\rho} + c\frac{\Delta\beta}{\beta}, \quad \text{..... (2.2)}$$

$$where\ a = \frac{1}{2cos^2\theta} = \frac{1 + tan^2\theta}{2}, b = 0.5 - \left[\left(\frac{2\beta^2}{\alpha^2}\right)sin^2\theta\right], c = -\left(\frac{4\beta^2}{\alpha^2 sin^2\theta}\right),$$

$$\alpha = \frac{\alpha_1 + \alpha_2}{2}, \beta = \frac{\beta_1 + \beta_2}{2}, \rho = \frac{\rho_1 + \rho_2}{2}, \Delta\alpha = \alpha_2 - \alpha_1, \Delta\beta = \beta_2 - \beta_1, \Delta\rho = \rho_2 - \rho_1$$

$$\Delta\theta = (\theta_i - \theta_I)/2, and\ \theta_t = \arcsin[\left(\frac{\alpha_2}{\alpha_1}\right)sin\theta_i]$$

Practically, the discrete reverberations of reflectivity of primary wave αα /Δ, S wave reflectivity ββ /Δ and fractional density variation ρρ /Δ on the reflection amplitude R(θ) are not observed. However, reflection amplitude variation as a function of angle of incidence is quite evident. Equation (2.2) can be otherwise expressed in series of angles of incidence as

$$R(\theta) = \left[\frac{1}{2}\left(\frac{\Delta\alpha}{\alpha} + \frac{\Delta\rho}{\rho}\right) + \frac{1}{2}\frac{\Delta\alpha}{\alpha} - 4\frac{\beta^2}{\alpha^2}\frac{\Delta\beta}{\beta} - 2\frac{\beta^2}{\alpha^2}\frac{\Delta\rho}{\rho}\right] sin^2\theta + [\frac{1}{2}\frac{\Delta\alpha}{\alpha}](tan^2\theta - sin^2\theta) \ldots\ldots\ldots.. \ldots (2.3)$$

We have three terms in equation (2.3). It was rearranged by Shuey (1985) in terms of Poisson's ratio rather than S wave velocity to give his well-known approximation, and was also rearranged by Wiggins (1987) at Mobil, and published by Gelfand and Larner (1986) as an approximation established on reflectivity of primary and shear waves.

The ratio of S wave to P wave velocity is thus defined as, 5 .0/ = αβ, then the third term in equation (2.3) becomes negligible,

$$R(\theta) = [\frac{1}{2}\left(\frac{\Delta\alpha}{\alpha} + \frac{\Delta\rho}{\rho}\right) + \left[\frac{1}{2}\frac{\Delta\alpha}{\alpha} - \frac{\Delta\beta}{\beta} - \frac{1}{2}\frac{\Delta\rho}{\rho}\right] sin^2 \ldots\ldots\ldots\ldots\ldots\ldots\ldots\ldots\ldots\ldots\ldots\ldots\ldots \text{(2.4)}$$

Letting

$$R_s \cong \frac{1}{2}\left(\frac{\Delta\alpha}{\alpha} + \frac{\Delta\rho}{\rho}\right) \ldots\ldots\ldots\ldots\ldots\ldots\ldots\ldots\ldots\ldots\ldots\ldots\ldots\ldots\ldots\ldots\ldots\ldots\ldots\ldots \text{(2.5)}$$

And

$$R_s \cong \frac{1}{2}\left(\frac{\Delta\beta}{\beta} + \frac{\Delta\rho}{\rho}\right), \ldots\ldots\ldots\ldots\ldots\ldots\ldots\ldots\ldots\ldots\ldots\ldots\ldots\ldots\ldots\ldots\ldots\ldots\ldots\ldots\ldots\ldots \text{(2.6)}$$

Equation (2.4) becomes

$$R(\theta) = R_p + (R_p - 2R_s)\sin^2\theta \, .$$

From the equation above we can get

$$R_s = \frac{R_p - G}{2} \ldots\ldots\ldots\ldots\ldots\ldots\ldots\ldots\ldots\ldots\ldots\ldots\ldots\ldots\ldots\ldots\ldots\ldots\ldots\ldots\ldots\ldots\ldots\ldots\ldots\ldots\ldots \text{(2.8)}$$

Where G=Rp-2Rs.

Thus we have the AVO attribute expression for the estimation of shear wave reflectivity. With the AVO intercept and AVO gradient G parameters provided, half of the difference between the two attributes can be used to define the shear wave reflectivity s R as shown in equation (2.8).

Shuey (1985) published a closed form approximation of the Zoeppritz equations which involved α, ρ and σ (Poisson's ratio)

$$R(\theta) = R_p + \left[R_p A_0 + \frac{\Delta\sigma}{(1-\sigma)^2}\right] sin^2\theta \frac{\Delta\alpha}{2\alpha}(tan^2\theta - sin^2\theta) \quad (2.9)$$

$$where\ \sigma = \frac{\sigma_1+\sigma_2}{2}, \Delta\sigma = \sigma_1 + \sigma_2, A_0 = B - 2(1+B)\frac{1-2\sigma}{1-\sigma}, and\ B = \frac{\frac{\Delta\alpha}{\alpha}}{\frac{\Delta\sigma}{\alpha}+\frac{\Delta\rho}{\rho}}.$$

With several assumptions, the equation above can be simplified as;

$$R(\theta) = R_P + Gsin^2\theta \quad (2.10)$$

The equation above is linear hence if we plot R as a function of Sin θ. A linear regression analysis on the seismic amplitudes to estimate intercept Rp, and gradient G is carried out. Prior to the linear regression, our data must be transformed from constant offset form to constant angle form.

Smith and Gidlow (1987) developed another approximation based on the Aki and Richards equation. They first rearranged equation (2.3) to get

$$R(\theta) = [\frac{1}{2}\left(\frac{\Delta\alpha}{\alpha} + \frac{\Delta\rho}{\rho}\right) - 2\frac{\beta^2}{\alpha^2}\left[2\frac{\Delta\beta}{\beta} + \frac{\Delta\rho}{\rho}\right] sin^2\theta + \frac{1}{2}\frac{\Delta\alpha}{\alpha} tan^2\theta \quad (2.11)$$

And then they simplified equation (2.11) by eliminating the dependence on density with Gardner's relationship

$$\rho = a\alpha^{1/4} \quad (2.12)$$

This can be differentiated to give

$$\frac{\Delta\rho}{\rho} = \frac{1}{4}\frac{\Delta\alpha}{\alpha} \quad \text{..... (2.13)}$$

Substituting equation (13) into equation (11) gives

$$R(\theta) = c\frac{\Delta\alpha}{\alpha} + d\frac{\Delta\beta}{\beta}, \quad \text{..... (2.14)}$$

$$where\ c = \frac{5}{8} - \frac{1}{2}\frac{\beta^2}{\alpha^2}sin^2\theta + tan^2\theta\ and\ d = -4\frac{\beta^2}{\alpha^2}sin^2$$

Using this equation, we can estimate Δα/α and Δβ/β by using generalized linear inversion (GLI). The GLI solution in matrix form is given by

$$\begin{pmatrix} \sum_i^N a_i^2 & \sum_i^N a_i b_i \\ \sum_i^N a_i\, b_i & \sum_i^N {b_i}^2 \end{pmatrix}\begin{pmatrix} \frac{\Delta\alpha}{\alpha} \\ \frac{\Delta\beta}{\beta} \end{pmatrix} = \begin{pmatrix} \sum_i^N a_i X_i \\ \sum_i^N b_i X_i \end{pmatrix} \quad \text{..... (2.15)}$$

The two variables Δα/α and Δβ/β, estimated by using the least squares solution given by equation (2.15), are fractional changes in P and S wave velocity. As such, they are related to P and S wave reflectivity, respectively. Also, the derivation of two other types of weighted stacks, the "Pseudo-Poisson's ratio reflectivity and the "fluid factor" by Smith and Gidlow (1987). Goodway et al. (1998) gave another way to approximate the fluctuation P and S wave based on transforming the Aki-Richards equation to the new variables Δ I*p*/I*p* and ΔI*s*/I*s*

$$R(\theta) = \left(\frac{1}{2}[1 + tan^2\theta]\right)\frac{\Delta I_p}{I_p} + \left[4\frac{\beta^2}{\alpha^2}sin^2\theta\right]\frac{\Delta I_s}{I_s} - [\frac{1}{2}tan^2\theta - 2\frac{\beta^2}{\alpha^2}sin^2\theta]\frac{\Delta\rho}{\rho} \quad \text{..... (2.16)}$$

Goodway et al. (1998) used a specific form of equation (2.16) to define the AVO attributes Δ I*p*/I*p* and ΔI*s*/I*s*. For a specific value of α/β = 2 and small angles of incidence for which tan θ = sin θ, the third term in equation (2.16) vanishes and equation (2.16) takes the form

$$R(\theta) = (1 + tan^2\theta)R_p - (2sin^2\theta)R_s \quad \text{(2.17)}$$

Following the approximation of the P wave and S wave fluctuation by using the generalized linear inversion (GLI) given by equation (2.15), the P wave and S wave impedance can be determined by integration. Furthermore, Goodway et al. (1998) estimated two additional AVO attributes in terms of Lame's constant calibrated by density λρ and μρ.

$$\lambda\rho = {I_p}^2 - 2{I_s}^2$$

$$\mu\rho = {I_s}^2$$

Comparison of the Approximations of Zoeppritz's Equation

We have several expressions for the linear approximation of Zoeppritz's equation, each with different significance. Bortfeld (1961) highlighted the fluid and rigidity terms which provided insight when interpreting fluid-substitution difficulties, Aki and Richard's equation highlighted the contribution of variations in the P- and S- wave velocities and density. Shuey, after learning about the contributions of Koefoed and the amplitude dependence on Poisson's ratio, decided to cast Aki and Richards's equation in terms of Poisson's ratio. One of the Shuey's main contributions is that he identified how various rock properties can be associated with near, mid, and far angle ranges. The first term is the normal-incident reflectivity on the right side of Shuey's equation, and this is constant across all angles of incidence. No significant contribution is made by the second term until incident angles of 15 degree or greater are reached. Shuey argued further argued the third term, is trivial and can be neglected if the range of incident-angle is below 30 degrees. The first and second term in Shuey's equation both have the normal-incident reflection coefficient. Verm and Hilterman (1995) modified Shuey's equation to emphasize the lithological characteristic is a function of incident angle:

$$R(\theta) = \frac{1}{2}\left(\frac{\Delta\alpha}{\alpha} + \frac{\Delta\rho}{\rho}\right)\left(1 - \frac{4\beta^2}{\alpha^2}sin^2\theta\right) + \frac{\Delta\sigma}{(1-\sigma)^2}sin^2\theta + \frac{\Delta\alpha}{2\alpha}(tan^2\theta - \frac{4\beta^2}{\alpha^2}sin^2\theta) \quad \text{(2.18)}$$

2.5 AVO Classification

Generally, the reflection coefficient curves classification as defined by Williams and Rutherford has become conventional and it is related to the classes of bright spot, phase reversal, and dim out established in the 1970s. The classification was modified for reflections within hydrocarbon saturated formations. According to Rutherford and Williams's classification, the slope of the reflection coefficient curve is negative for all classes (Figure 2.7). The reflection amplitude decreases in relation to the incident angle. Nevertheless, the non-relative amplitude can increase in relation to the incident angle as shown for both Class 2 and 3 AVO gas saturated anomalies. The discovery of slowly decreasing amplitudes with offset due to specific Class 3 AVO gas saturated anomalies was made by Castagna et al. (1998). There were named Class 4 AVO anomalies. Although, the main characteristic attribute for the Class 4 anomalies is still the high amplitude linked to the presence of hydrocarbon.

Properties of Class 1 Anomalies:

(i) Decreasing amplitudes with increase in angle, and there is possibility of phase reversal on the far angle stack

(ii) Amplitude on the full stack is lesser for the hydrocarbon zone than for an equivalent wet saturated zone.

(iii) Nature of wavelet is likely be peak-trough on the far angle stack or not.

(iv) Nature of wavelet is peak-trough on near angle stack.

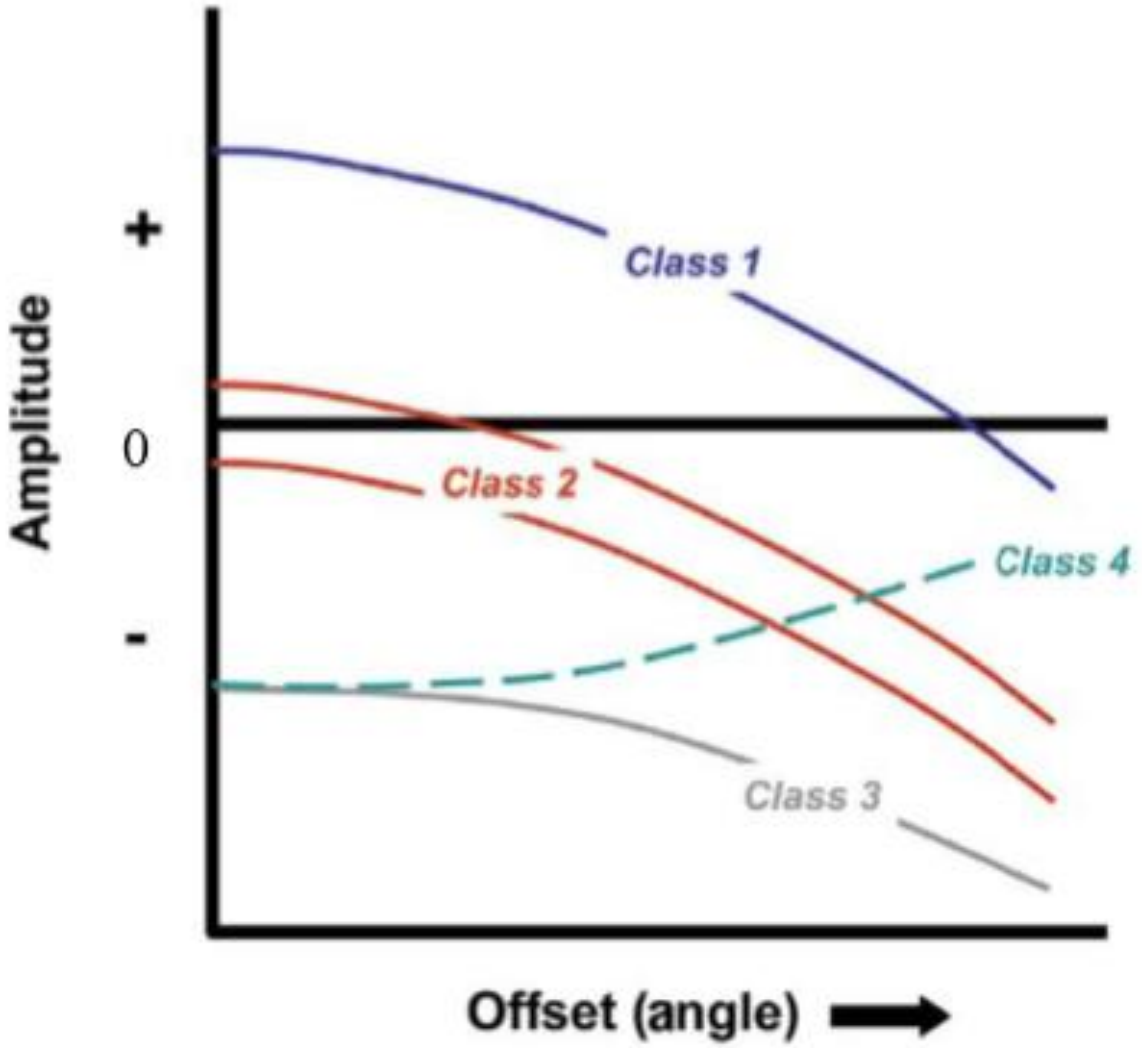

Figure 2.7 Classification of AVO Responses Class 1, Class 2, Class 3, and Class 4. (Hanafy, Said et al. (2014).

Properties of Class 2 Anomalies:

(i) The indicator of the gas sand on the near angle stack is minute.

(ii) As the angles increase, the amplitude of gas sand event increases. This attribute is more prominent than expected due to the decreasing amplitude of the shale upon-shale reflections.

(iii) It is possible the event of gas sand likely to be or not evident on the full stack, dependent on the influence of far angle amplitude to the stack.

(iv) Nature of the wavelet on the stack may or may not be trough-peak for a hydrocarbon charged thin bed.

(v) Wavelet appears as trough-peak on the far angle stack.

(vi) It is inferred that the rock types are within in the amplitude variation with angle of incidence.

(vii) AVO is unable distinctively a clean wet sand from a gas sand, because they both have increasing behavior with offset.

Properties of Class 3 Anomalies:

(i) Regions saturated with hydrocarbon appear bright on the stack section including on all angle limited stacks.

(ii) The hydrocarbon reflection amplitude, in relation to the surround reflection amplitude increases moderately with incident angle range. Although the amplitude of the hydrocarbon event can decrease with angle.

(iii) The presiding phase of the seismic wavelet is zero and the tuning extent is above the reservoir which is due to the fact that the wavelet appears trough-peak on all angle stacks.

(iv) Prediction of hydrocarbon from stack section is feasible

2.6 Limitations of the AVO

The Zoeppritz equation considers only the elastic properties of the rocks ignoring the non-elastic properties such as velocity dispersion attenuation. Considering these factors, the AVO technology is still very much limited. As different lithologies may exhibit distinct Poisson's ratios and gas bearing strata usually exhibit anomalously low Poisson's ratios. According to Castagna 2014, AVO has proven that it could be a prospective seismic lithology tool and direct hydrocarbon indicator. However, experience has shown that the theoretical potential for AVO analysis is, most times has not been achieved in practice. Altogether, AVO analysis has proven to be unsuccessful in some other areas, perhaps with a different type of geology and this is a limitation to this method.

CHAPTER THREE

METHODOLOGY

3.0 Introduction

The materials and methods employed in the determination of subsurface rock properties from AVO analysis in the OTG field, Niger Delta are outlined in this chapter.

3.1 Processes and Workflow

Figure shows the summary of the processes and the workflow carried out in this research.

3.2 Available Data Set

The seismic data used for this study includes pre-stack seismic data with far, near offset gathers, a full stack gather was also provided alongside wireline logs for five wells (wells OTG 01 - 05), seismic base map, each well comprises a compressional sonic log, shear sonic log, gamma ray log, bulk density, resistivity log. The available wells in the field were screened for their suitability for the AVO analysis and forward modelling. The depth referencing and well deviation surveys were checked for consistency and accuracy. The depth was referenced to true vertical depth subsea.

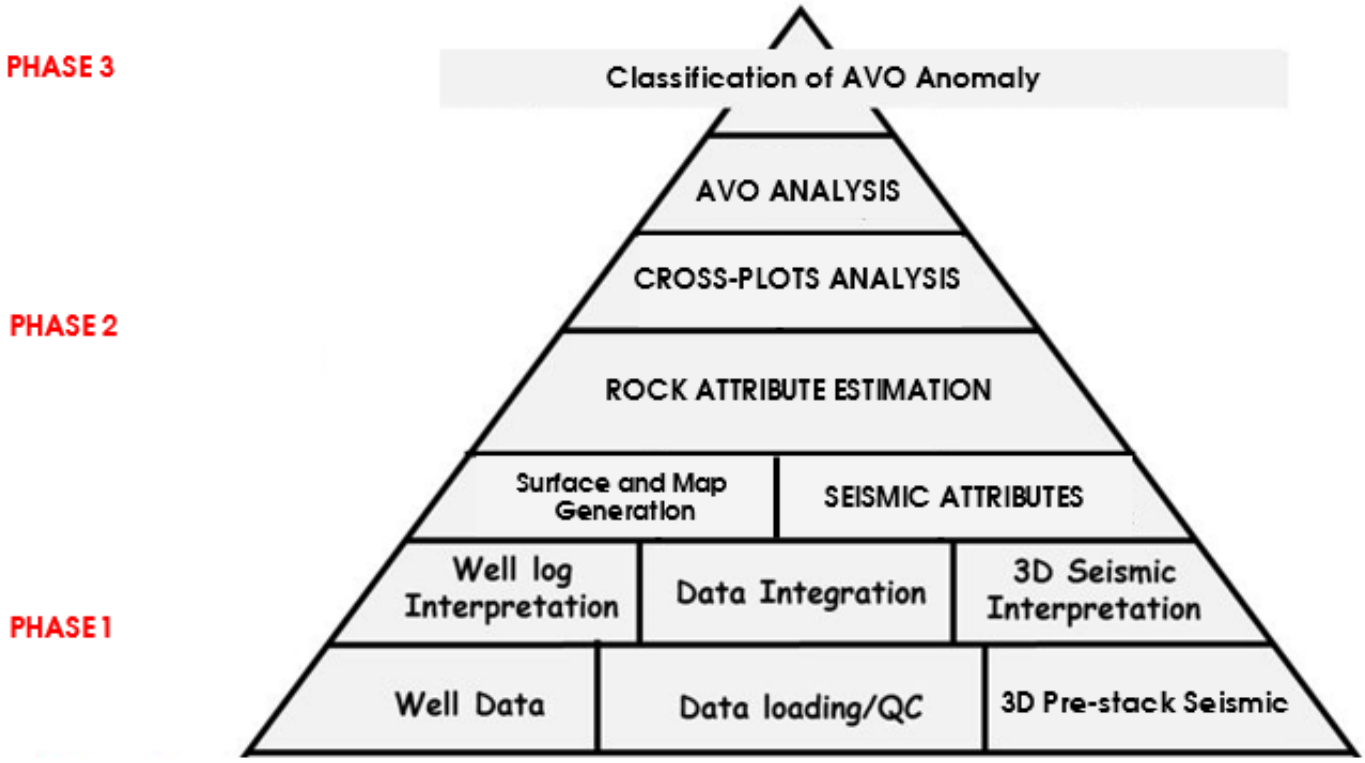

Figure 3.1 Workflow showing the methodology.

Table 3.1 Table showing all the available logs in the data set

WELL NAME	CALIPER	GAMMA	RESISTIVITY	NEUTRON	DENSITY	CHECKSHOT	SONIC
OTG 01	+	+	+	+	+	+	+
OTG 02	+	+	+	+	+	+	+
OTG 03	+	+	+	+	+	+	+
OTG 04	+	+	+	+	+	+	+
OTG 05	+	+	+	+	+	+	+

3.3 Data Interpretation

3.3.1 Data QC and Loading

The pre-stack seismic data and available logs were quality checked and loaded into the Petrel software for interpretation, the check shot was also loaded alongside for the well-to-seismic tie to be done later in the workflow. Figure 3.2 shows the location of our wells on the base map and Figure 3.3 shows the 3D view of the seismic volume and loaded wells.

3.3.2 Well Correlation

The logs were displayed and arranged in the north to south direction within the study area on the well section window (figure 3.4a), then a lithological correlation was carried out using gamma ray log. The resistivity log was used to delineate the reservoirs with potential hydrocarbon saturation. Three reservoirs namely OTG Sand 1-5 were correlated across the wells. As seen in the figure below, the wells were correlated according to position in the base map and were correlated in the north to south direction as shown below (figure 3.4b).

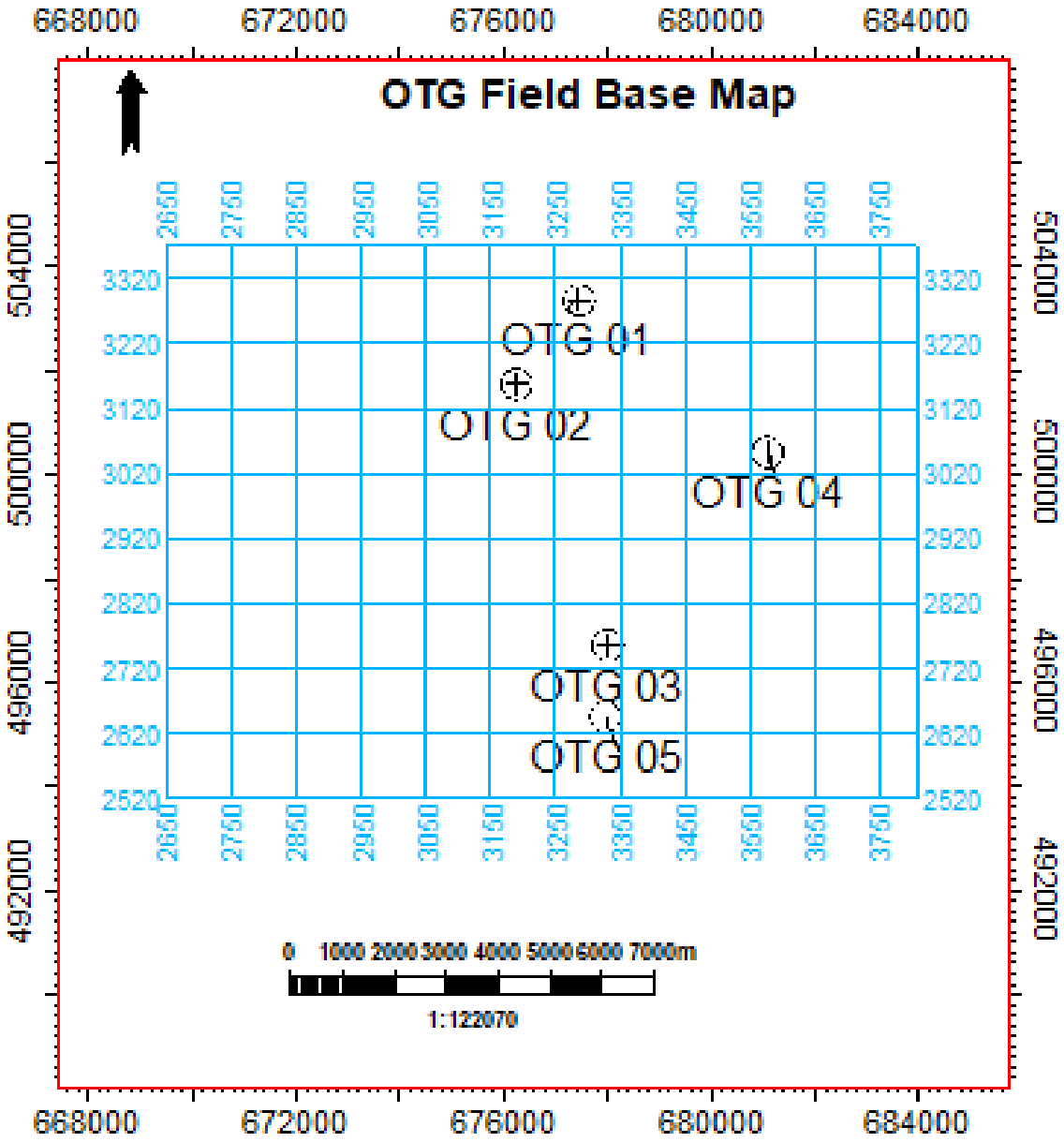

Figure 3.2 OTG Field Base Map

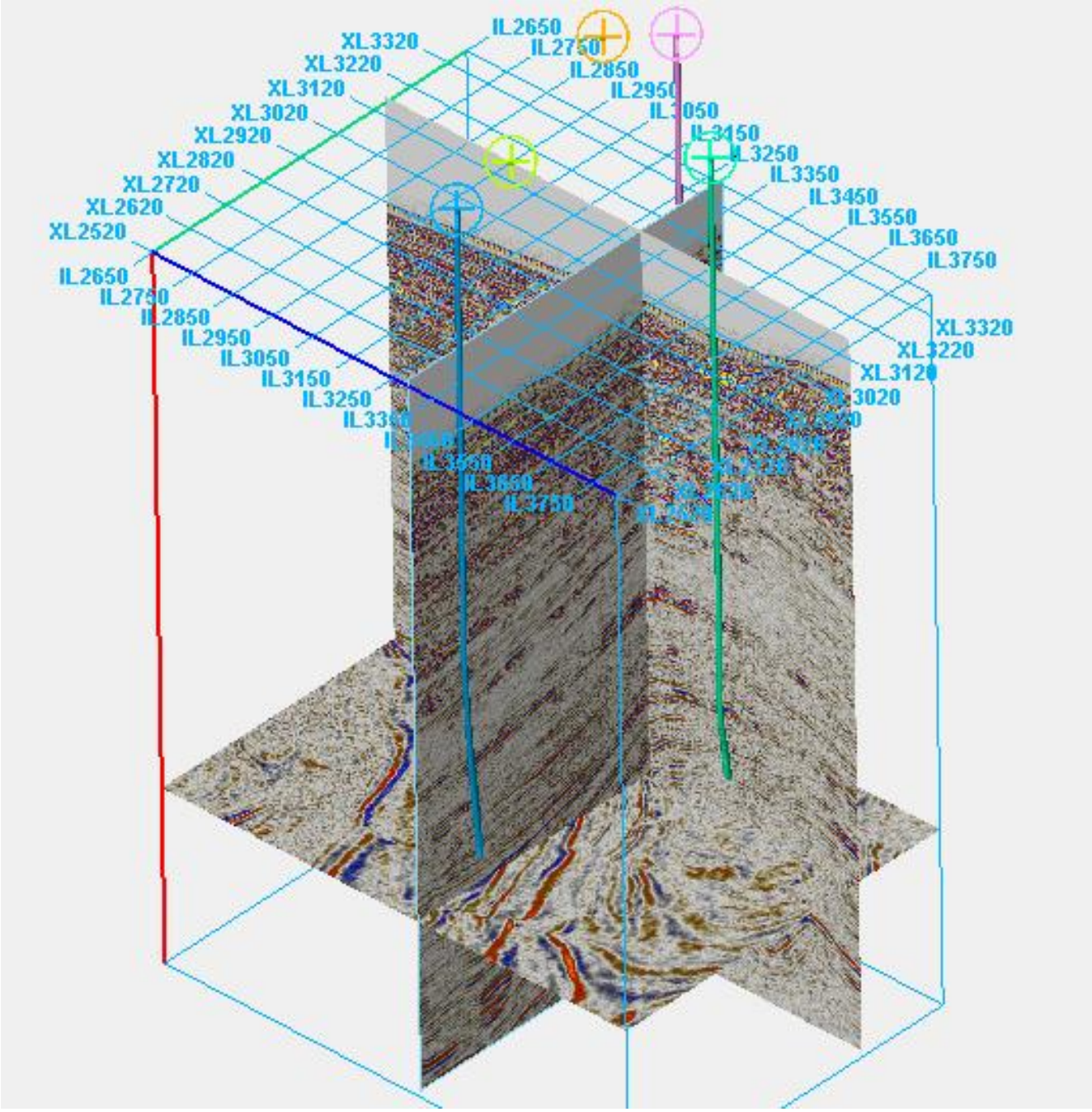

Figure 3.3 Seismic 3D volume and wells

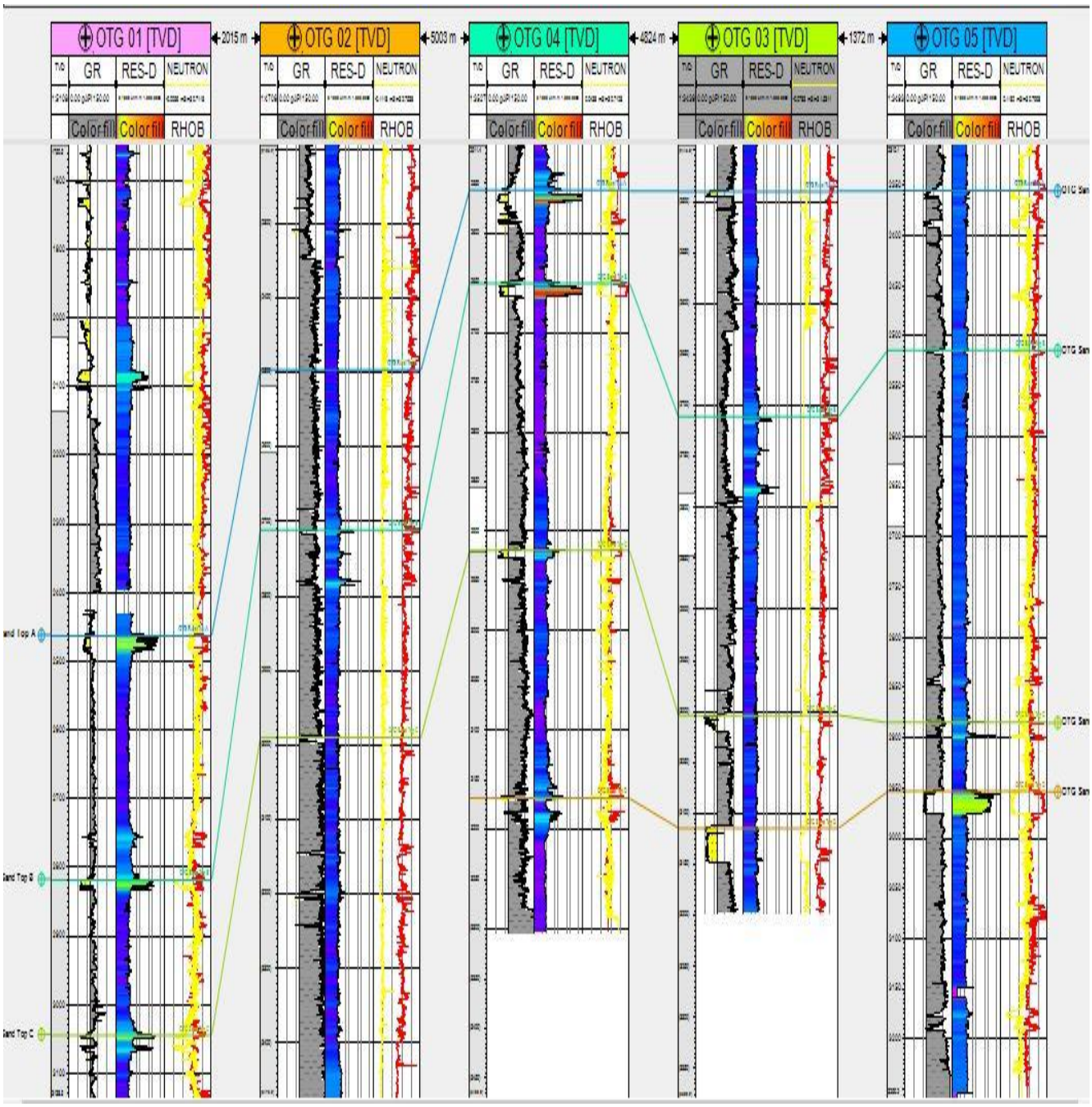

Figure 3.4a Well Section showing Lithological Correlation across all wells.

.

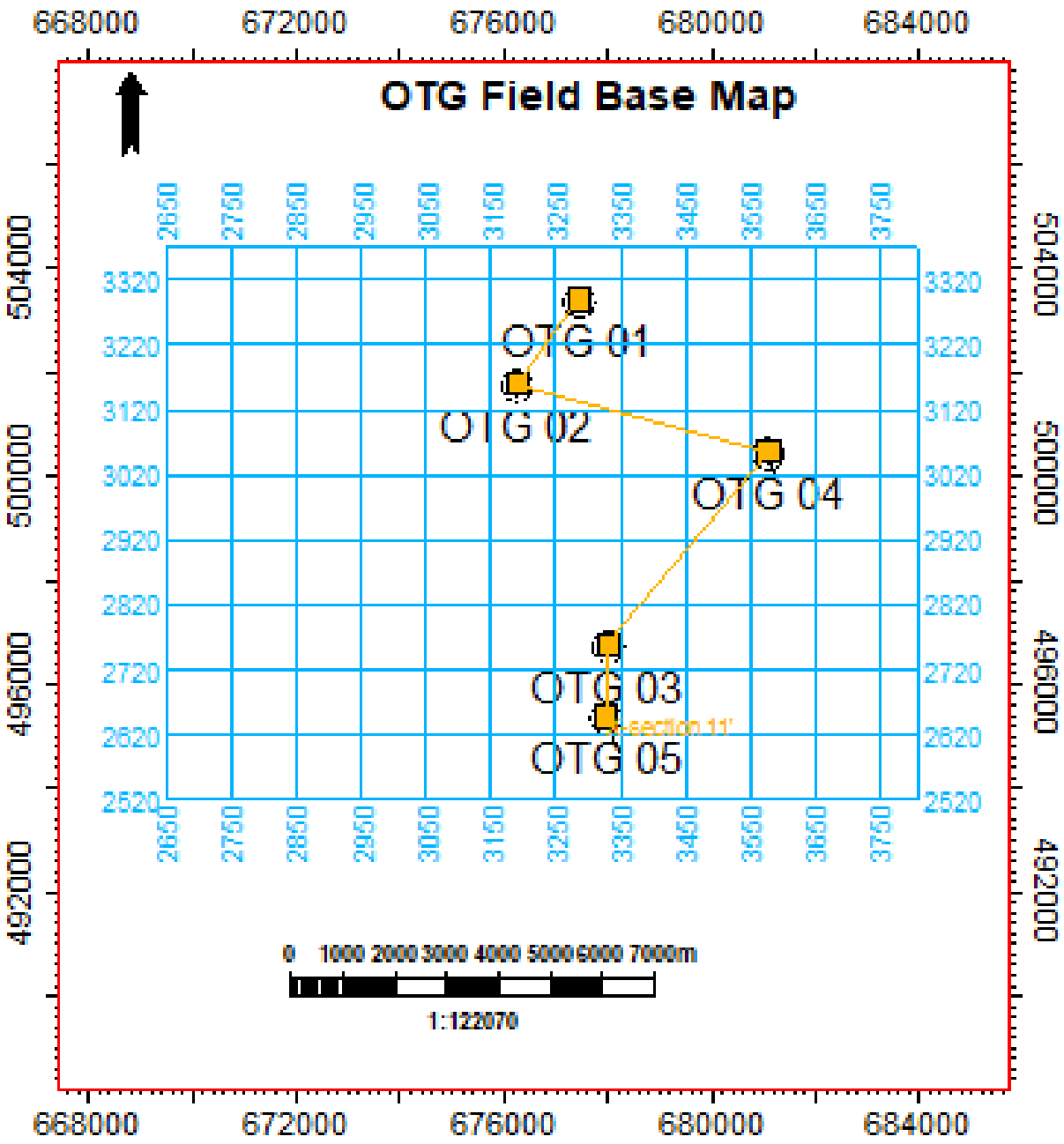

Figure 3.4b: Base Map showing direction of Well Correlation

3.3 Well to Seismic Tie

A time depth relationship was computed by integrating the slowness function measure at a wellbore. Using the well logs (bulk density and P-sonic) thus the acoustic impedance was computed. The earth reflectivity coefficient generated which was convolved in this case with the extracted wavelet was used to generate a synthetic seismogram at the well location as shown in figure 3.6 below. The generated synthetic had a relatively precise correlation with the original seismic with the top of reservoir – OTG Sand Top B falling on the peak(red). This is a fundamental step in seismic interpretation, it relates subsurface measurements obtained at borehole measured in depth and seismic data measured in time. It helps to compare what we see on the seismic data compared to the synthetic.

3.3.5 Horizon Mapping

After the correlation of possible reservoir from the qualitative interpretation from the well section and well to seismic tie, it is much easier to display the wells on seismic section and locate the top of the mapped reservoirs on seismic. These horizons were mapped across the 3D volume as shown in figures 3.6, 3.7a and 3.7b respectively to estimate reservoir thickness and select the suitable reservoir for the AVO analysis later on and also generate surfaces.

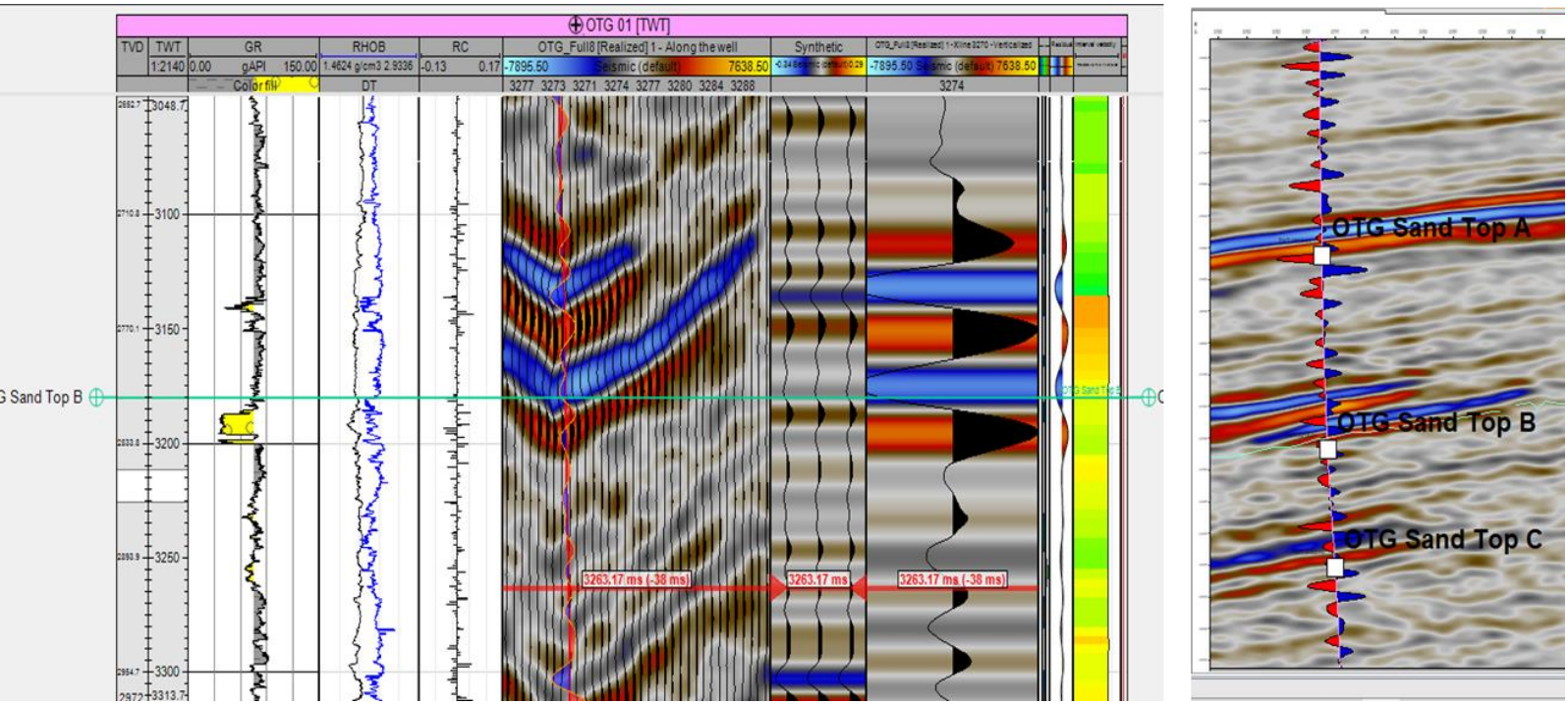

Figure 3.5 Seismic Section showing the horizons mapped across the seismic volume.

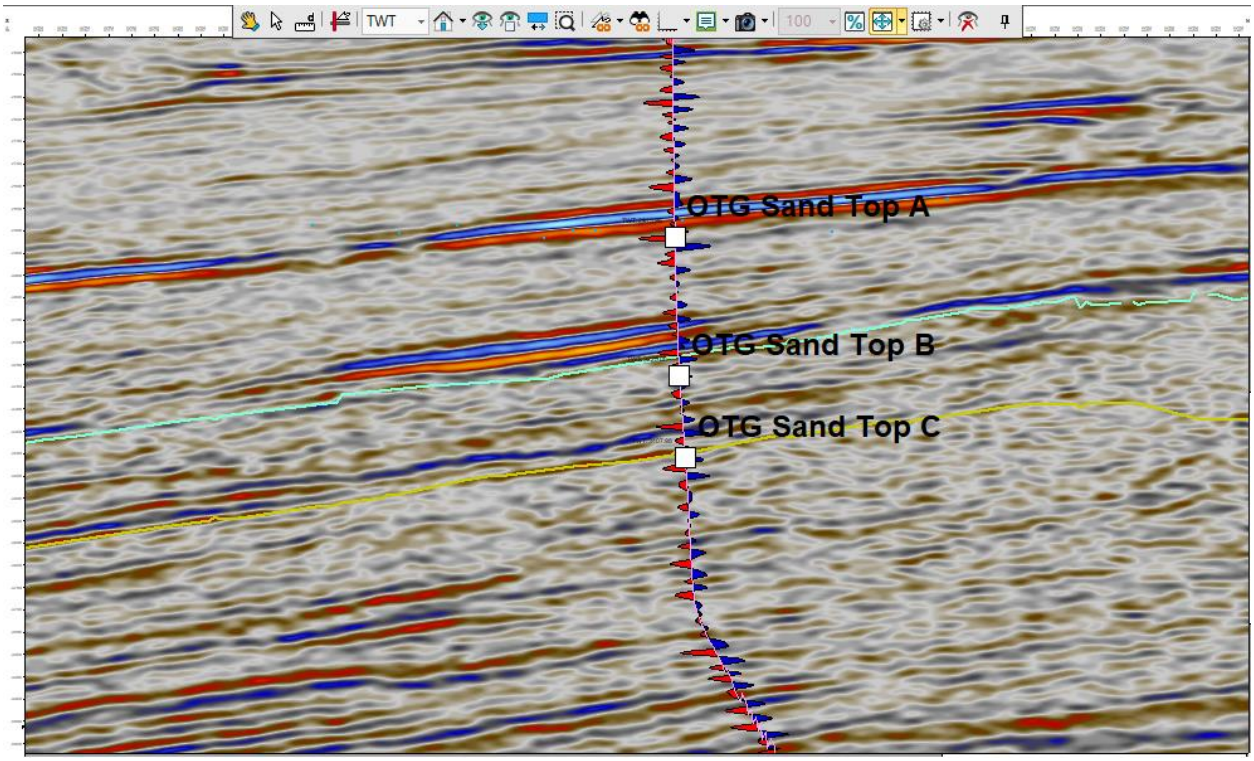

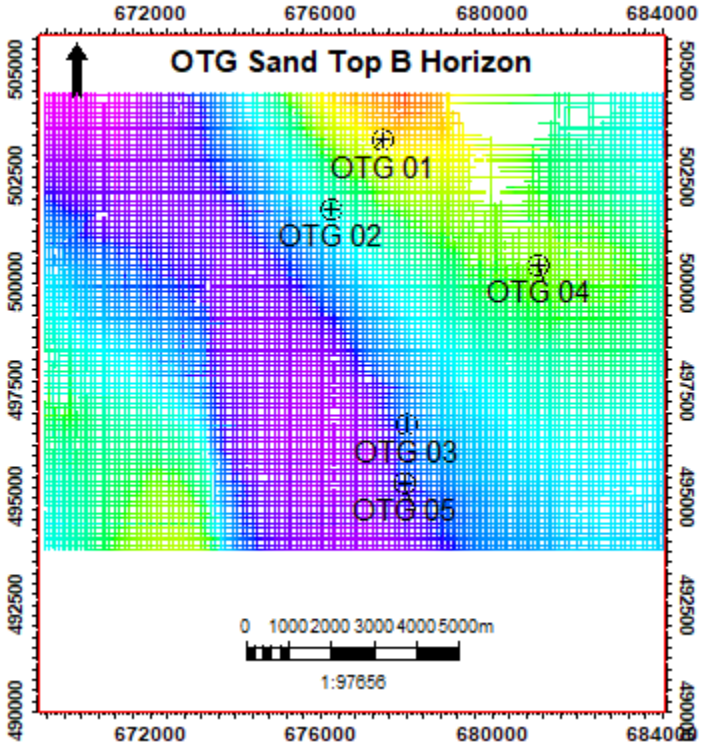

Figure 3.6 Seismic Section showing the horizons mapped across the seismic volume.

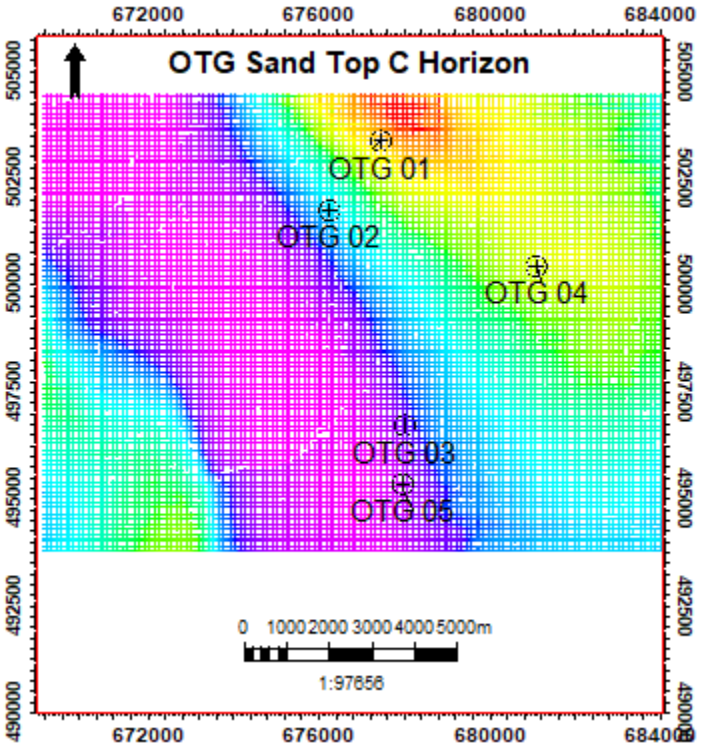

Figure 3.7a OTG Sand Top B Horizon

Figure 3.7b OTG Sand Top C Horizon

3.3.7 Data Export to Hampson Russell

After interpretation on Petrel, the well tops and mapped horizons were exported from Petrel to Hampson Russell for rock physics and AVO analysis.

3.4 Rock Physics and AVO Analysis

3.4.1 Subsurface rock properties obtained

Several rock properties were derived from the available logs within the data set, which in turn was used as fluid prediction tools, in this case the fluid being gas. Such properties include; P-wave velocity, S-wave velocity, Poisson's ratio, Acoustic impedance.

3.4.2 S-wave velocity

The velocity of S wave was derived from the shear wave sonic log (dTS) in Petrel. The S-wave speed Vs, depends on the shear modulus and the density. Even though they are slower than P-

waves, the S-waves still has considerable velocity. An essential unique characteristic of S-wave is its inability to propagate through fluid because fluids cannot transmit a shear stress. The knowledge of this behavior was useful in the prediction of the nature of fluid saturating the reservoir. This is deduced when S wave velocity is plotted against other rock parameters.

3.4.3 Acoustic Impedance

The difference in acoustic impedance between rock layers affects the reflection coefficient. Hydrocarbon saturated sands have lower acoustic impedance which are usually encased by units of higher acoustic impedance, while non-hydrocarbon clastic hard rocks have higher acoustic impedance than their overlying units. In the light of these highlighted rock properties, our target horizon exhibits a Poisson's ratio change in the range above 0.4 which is typical of brine.

3.4.4 P-wave/S-wave Cross plot for Castagna's Equation

In rock physics and petrophysics, the mud rock line, also called Castagna's equation or Castagna's relation, is an empirical linear relation between seismic P-wave velocity and S-wave velocity in brine-saturated siliciclastic rocks (i.e. sandstones and shales).

The equation reads:

$$\mathbf{V_p = aV_s + b} \quad \ldots\ldots\ldots\ldots (3.1)$$

In this research, the velocities of the P wave and the velocities of the S wave were extracted from the wells and subsequently plotted against each other (figure 3.8) to compute the values for a and b in the Castagna's equation to arrive at a reasonable well-seismic correlation. The derived a and b values from our cross plot are 1.1251 and 1229.6 respectively.

Selecting the seismic and correlating the well

The seismic data is needed for these steps in the AVO modeling workflow:

(1) To extract a wavelet.

(2) To correlate the well, i.e., to optimize the depth-time relationship between well and seismic.

(3) To compare with the resulting synthetic seismogram.

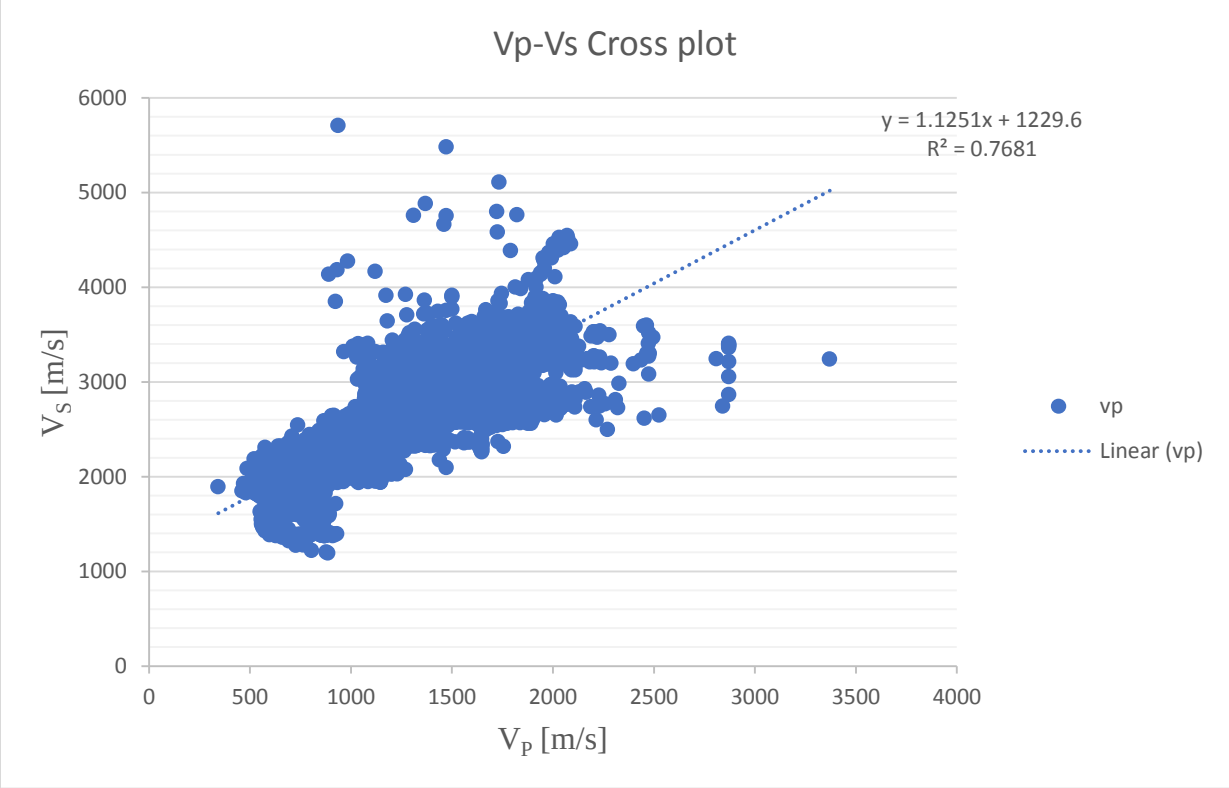

Figure 3.8 Vp-Vs Cross plot to estimate values of a and b for Castagna's equation

3.4.5 Wavelet Extraction

Using statistical approach, a wavelet was extracted from angle gathers for the near offset. An average zero phase wavelet was generated using these two wavelets for the seismic to well data correlation.

There are two basic methods for extracting the wavelet. One method uses the wells, and can give a good estimate of both amplitude and phase spectra of the wavelet. However, that method cannot be used until the well is correlated, i.e., until the proper depth-time relationship has been determined.

The second method – called “statistical” – uses the seismic data alone to extract the wavelet as shown in figure 3.15. This will evaluate the amplitude spectrum from the seismic data; however, assumption was made about the phase – typically assuming the data are zero phase. In this step, we extracted a statistical wavelet. The wavelet extraction was processed and rarefied using the wells subsequently. The extracted wavelet is shown in the figure 3.16.

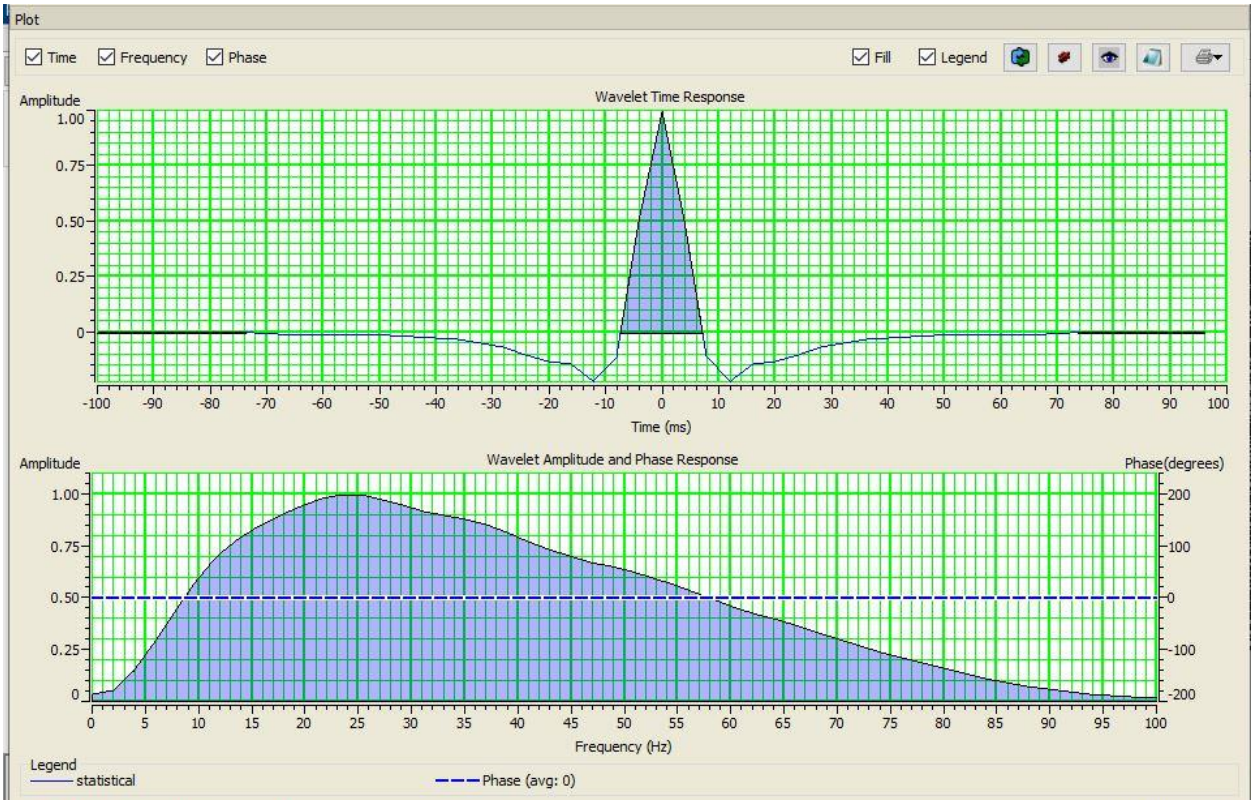

Figure 3.9 Extracted Wavelet from Seismic

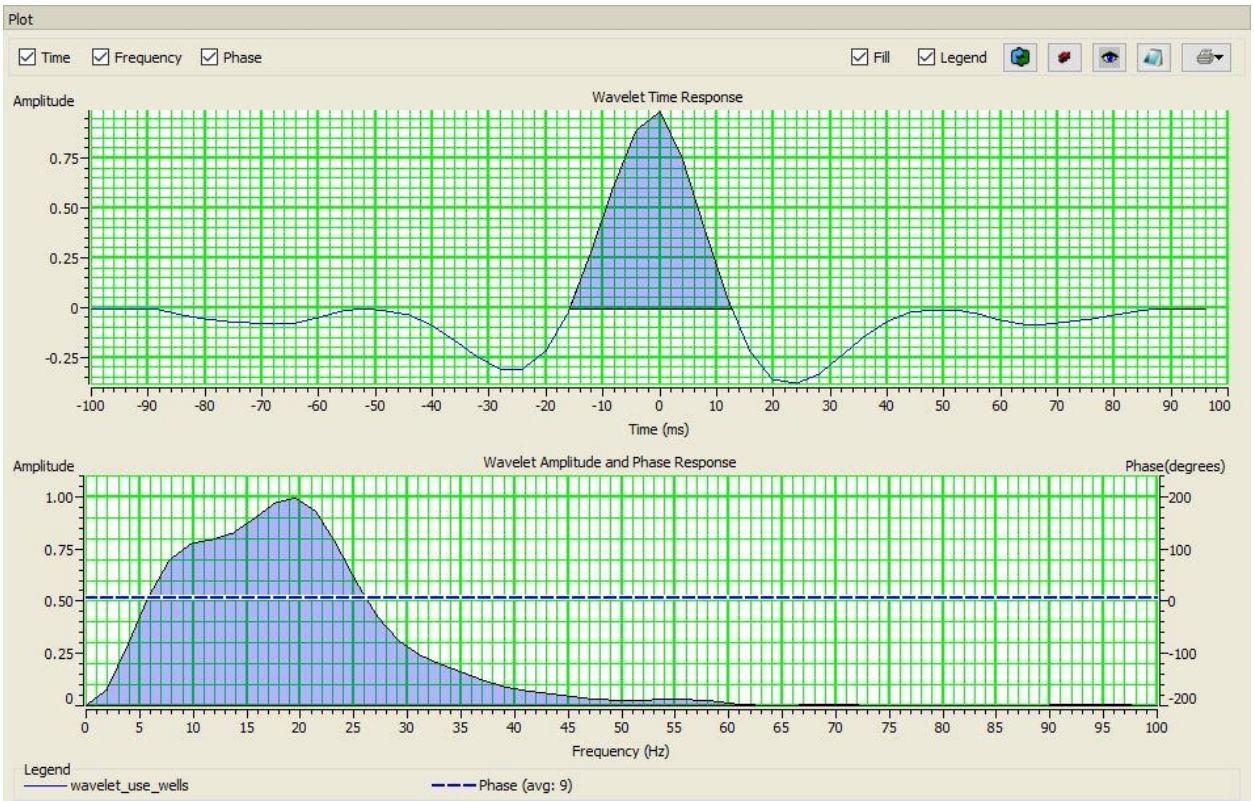

Figure 3.10 Extracted Wavelet from Wells

3.4.6 Log Correlation

This process involved evaluating the current depth-time conversion and optimizing it so that the derived synthetic matches the seismic optimally (Figure 3.11). This is necessary because the depth-time curve derived from the input sonic log is rarely sufficient for that purpose.

3.4.7 Identifying scenarios and creating synthetics

The next step in the Workflow was to Extract wavelet using wells. This process was carried out within the Log Correlation Window. The zero-phase statistical wavelet was used here to identify scenarios.

One scenario was chosen – the in-situ scenario which is present in the logs. In addition, up to 4 other scenarios were modelled. In the figure 3.19, Pure Oil and Pure Brine were selected, as well. Note that in addition to specifying pure hydrocarbons, a combination of the three components was specified using the Ternary diagram. The well display was modified to show the 3 scenarios for each of the P-wave, S-wave, Density, and Poisson's Ratio curves.

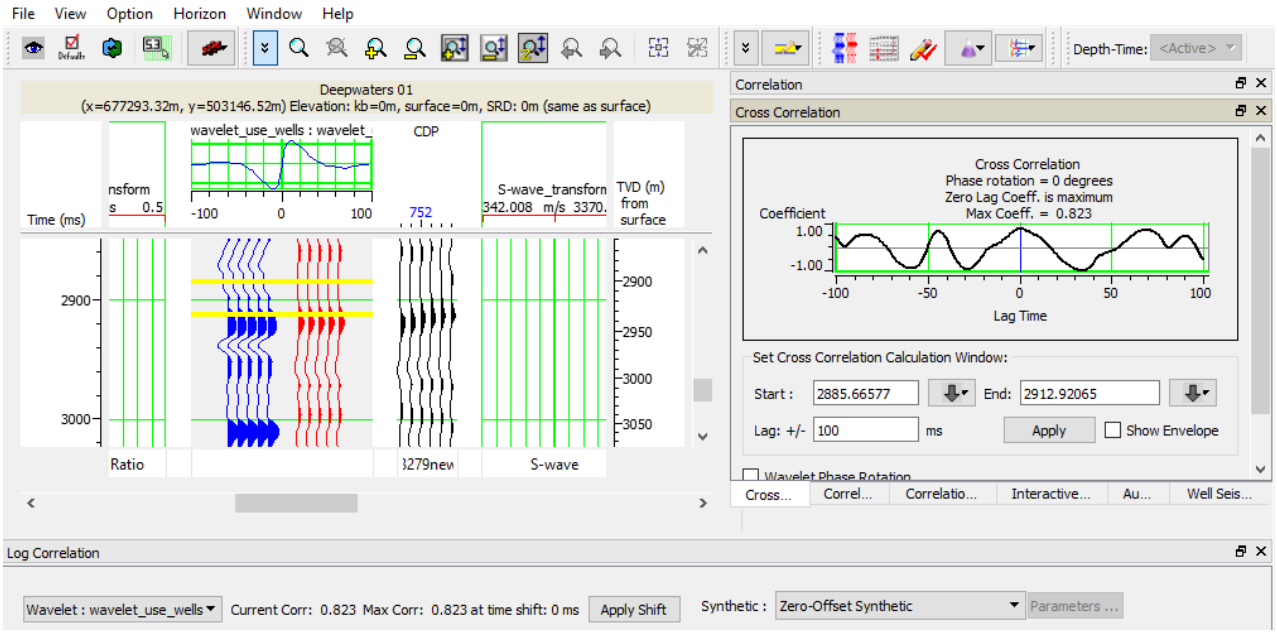

Figure 3.11 Well to Seismic Correlation Window in Hampson Russell

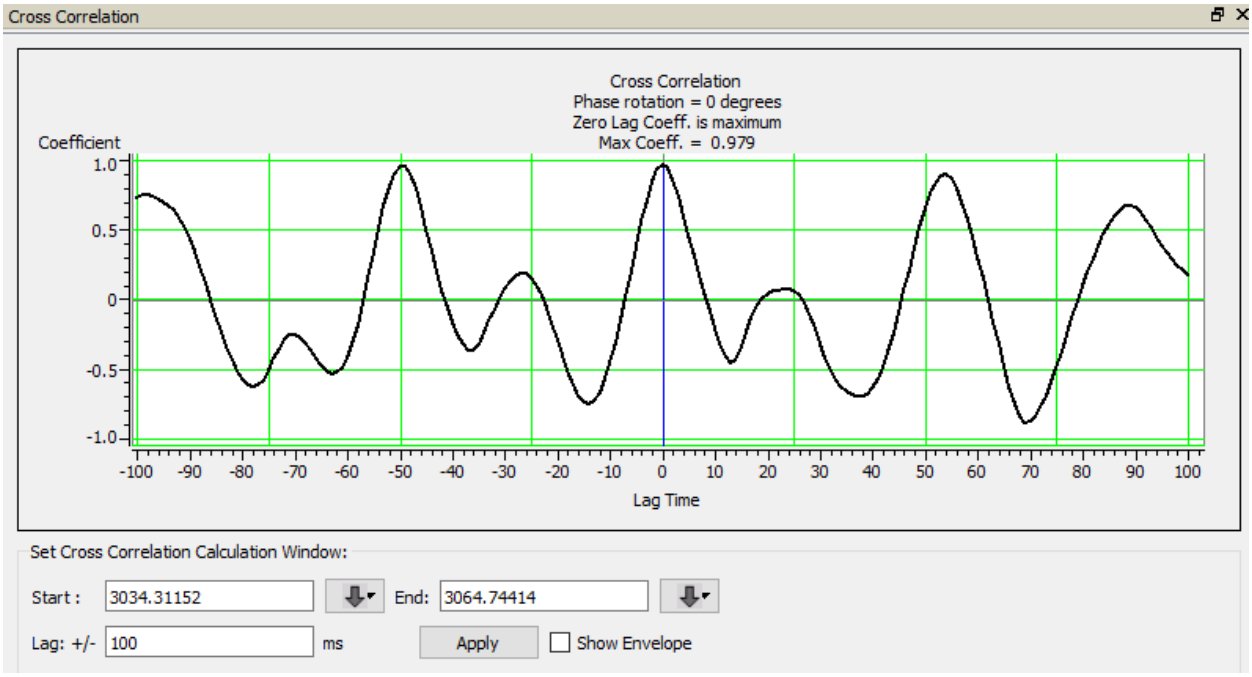

Figure 3.12 Cross-Correlation Window

3.4.8 Super Gather

This process was done on the input seismic data. Super Gather is the process of forming average CDPs to enhance the signal-to-noise ratio. The averaging was done by collecting similar offset traces within adjacent CDPs and adding them together. This process reduces random noise, while maintaining amplitude versus offset relationships (figure 3.13). This means that 3 adjacent CDP's will be summed to give each output CDP. This was done to reduce random noise.

3.4.9 Trim Statics

Trim Statics is the process which attempts to correct for residual moveout errors and align the events on the gathers. There are a number of reasons why this process is necessary, including errors in velocity analysis, and non-hyperbolic moveout. Whatever the cause, these residual moveout errors can cause significant distortions to the calculated AVO attributes, so they need to be corrected before proceeding. In the Trim Statics process, a pilot trace is formed by stacking each CDP gather. Then, each gather trace is correlated with the pilot trace, using a series of sliding windows. The cross correlations are used to calculate an optimal time shift for that window. Finally, the shifts for the windows were interpolated to produce a time-variant stretch of the trace. The result is to align events with the pilot trace. The resulting section is displayed below (figure 3.14)

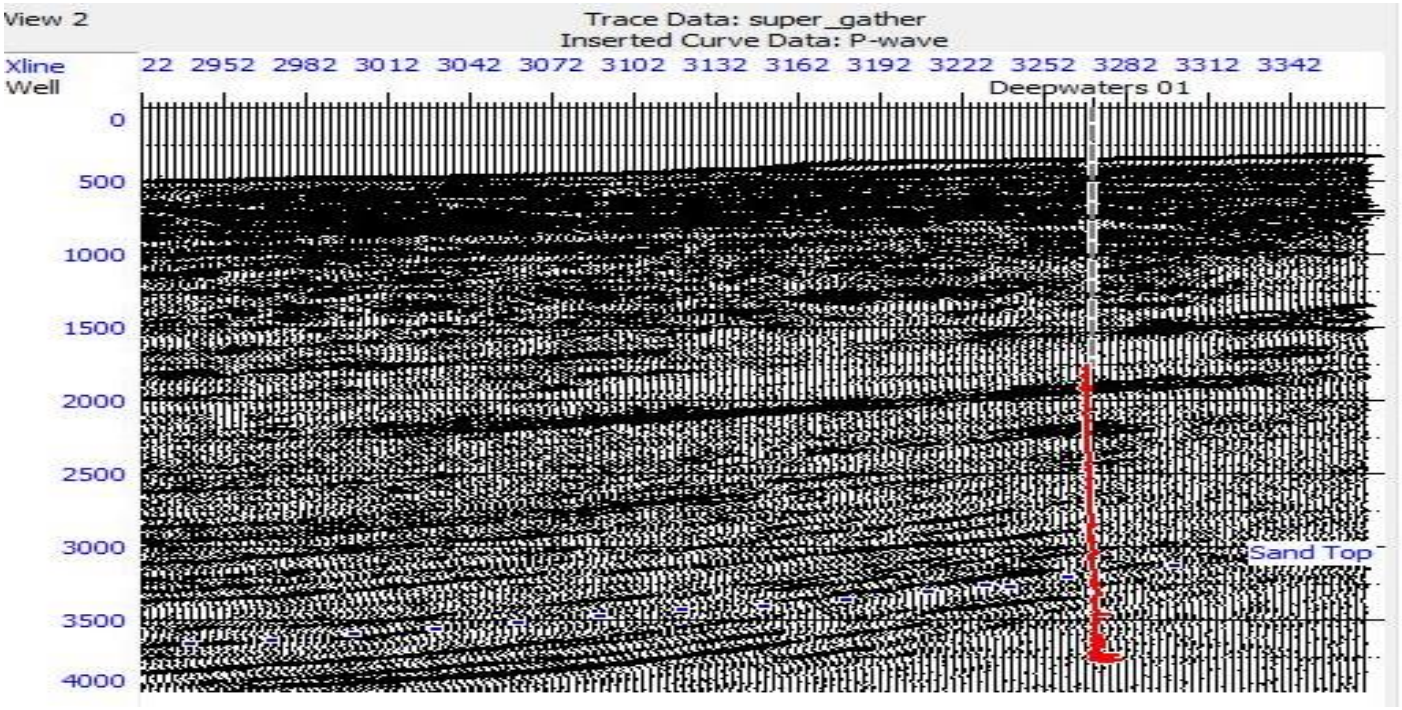

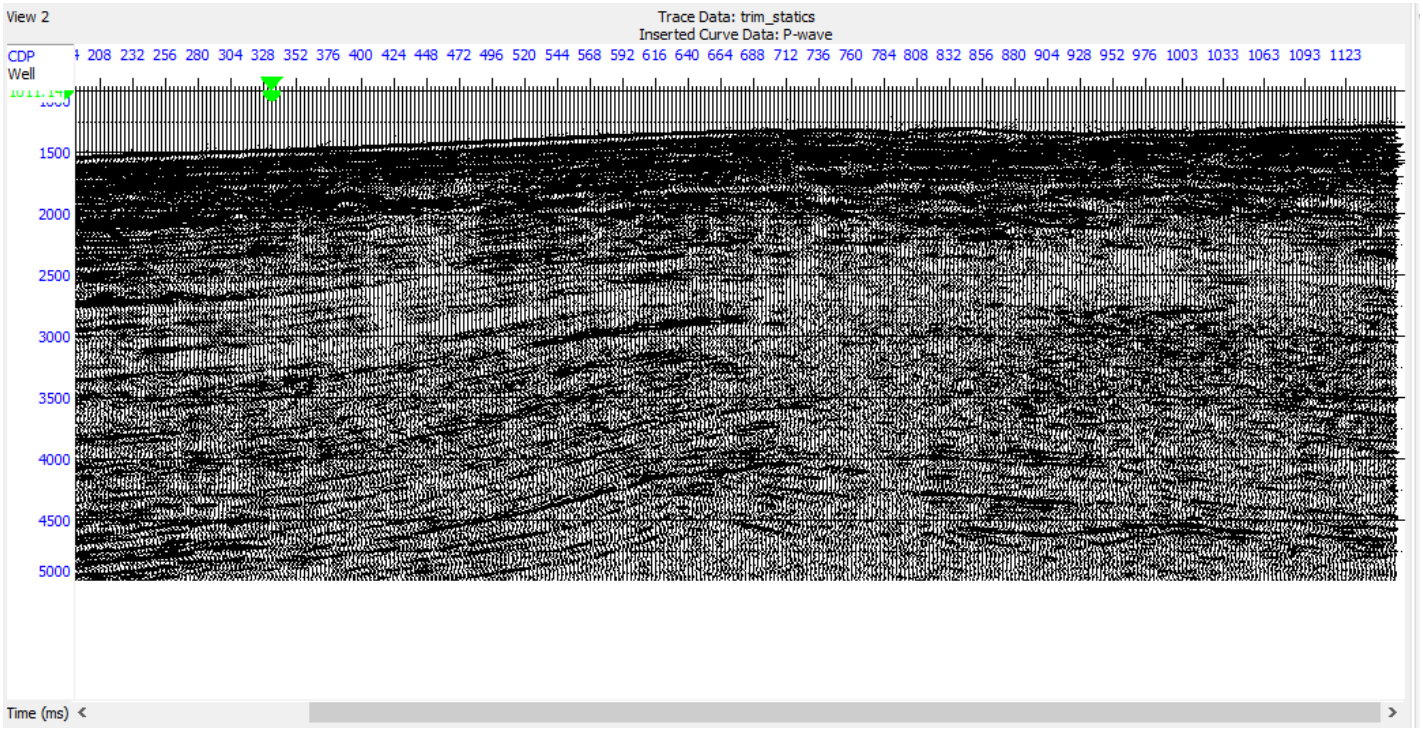

Figure 3.13 Seismic section showing the super gather

Figure 3.14 Seismic section showing trim statics output derived from super gather

3.4.10 Setting Up Velocity Model

A velocity model was set up which we used for all subsequent angle calculations. A single log was used from the well, with a 500 m smoothness and a sample interval of 0.2m:

Angle Gather:

This process involved the change from offset to the angle domain (figure 3.15) From the display from the super gather colored volume, our angle was about 5 degrees, velocity field set up initially was used for this process.

3.5 AVO Analysis

Deterministic AVO analysis was carried in Reservoir 1 with OTG Sand 01 to study the offset-reflectivity of gas sands in the area. Similar study was carried out in the same well OTG 01 but on another reservoir 2 to also see if it depicted characteristic AVO response.

The S-wave log was created using Castagna's mud rock equation, which relates S- and P-wave velocities. The resulting Poisson's ratio log is shown. Castagna's equation was used to calculate the correct shear-wave velocity for the layer at this water saturation. The synthetic was created using the P-wave sonic log, the created S-wave log and the density log. The created synthetic seismogram showed clear AVO effects at approximately the same depth with the real seismic data. That is, events in the synthetic seismogram match the original seismic data. Also, the data was amplitude preserved thus fit for AVO studies. To remove long unwanted offset and early arrivals which might distort the AVO signal. For the data to be suitable for AVO studies, the angle of incidence was tested for by plotting RMS velocities or P-wave on the seismic data. It was found that the data contained angles of incidence between 0 and 17 degrees. Super gather was done to enhance the signal-to-noise ratio, this was done by averaging adjacent CDPs and

adding them together. The number of offsets was set to 20 and the rolling parameters was set to five cross lines and five In-lines after super gather, the events were more visible and aligned. Angle gather was then created and the events were well aligned. The P-wave log was used as input velocity and a smoothening of 500 ms was applied after the angle gather have been created. To make the detection of hydrocarbon an easy task, the AVO data must be interpreted correctly. A gradient analysis was done on the real data to determine the shape of the curve which would help in the classification of the anomaly.

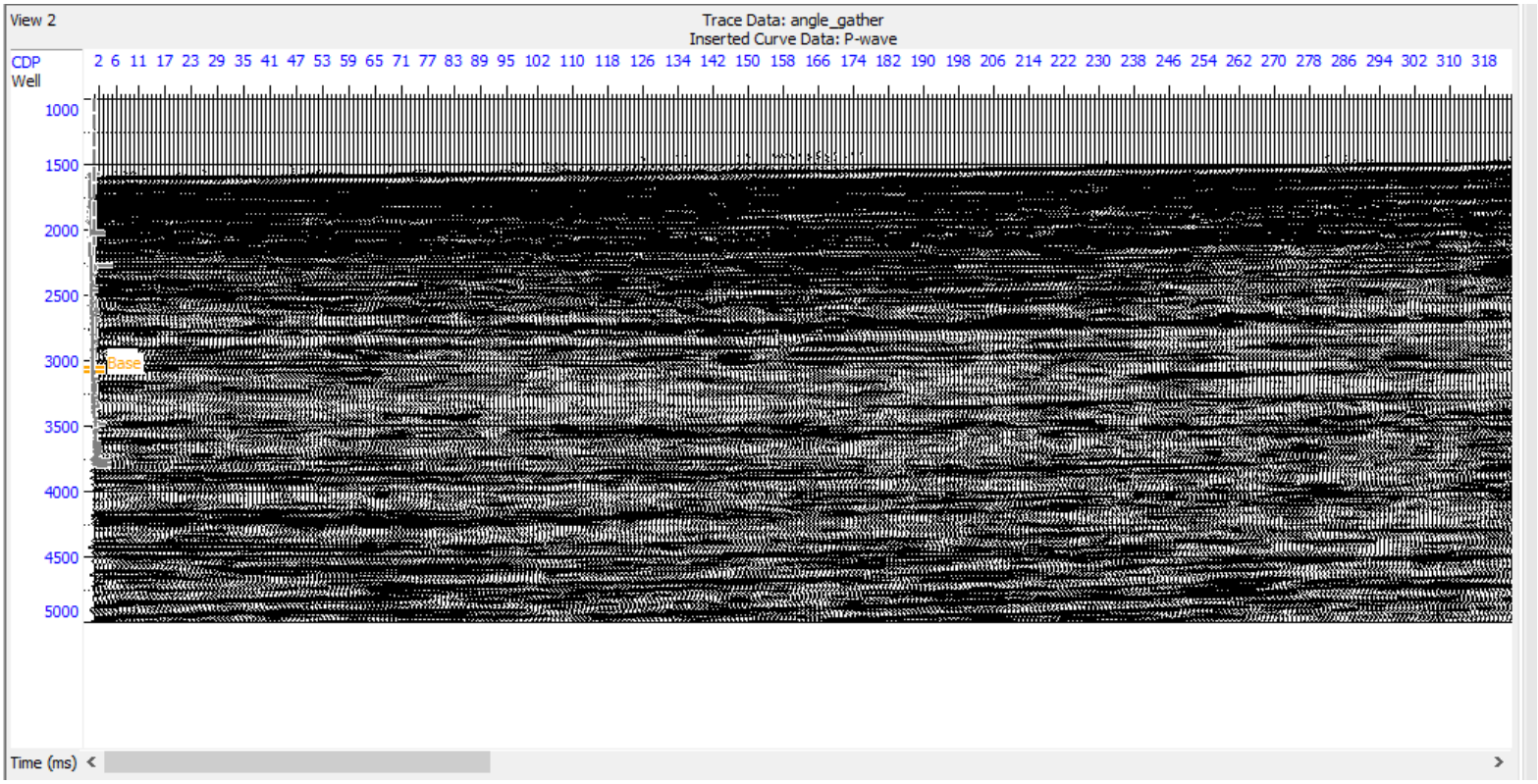

Figure 3.15 Seismic sections showing the angle gathers

Chapter Four

Results and Discussion

Qualitative Well Log Interpretation

From the gamma ray log several reservoirs were identified, furthermore, using the resistivity log, reservoirs with potential hydrocarbon saturation were delineated and correlated across the five wells; however, two reservoirs, figure 4.1 and figure 4.2 were selected from the OTG well 01 due to the likely presence of gas in these reservoirs. This observation was made by a qualitative study of the logs (gamma, resistivity and neutron/porosity). The presence of gas in these reservoirs makes them suitable for this study hence their selection.

Surface Generation

Having mapped the horizons of the reservoirs across the seismic volume. Time surfaces were generated from the mapped horizons as illustrated in Figure 3.10a and Figure 3.11a and converted into depth maps with a derived velocity model from the sonic logs, depths maps are displayed below in figures 3.10b and figure 3.11b.

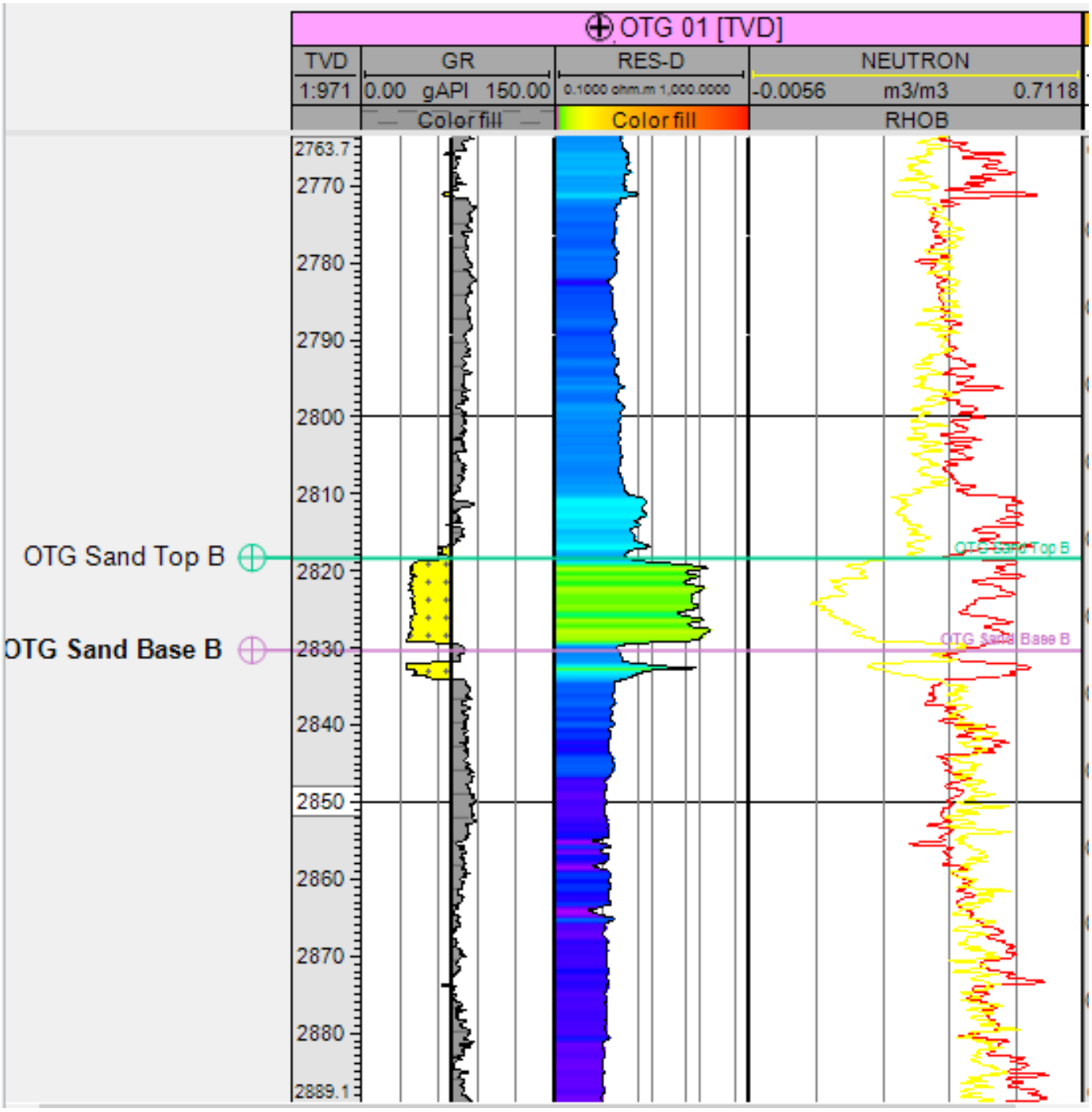

Figure 4.1 Well Section for OTG Sand Top B Reservoir

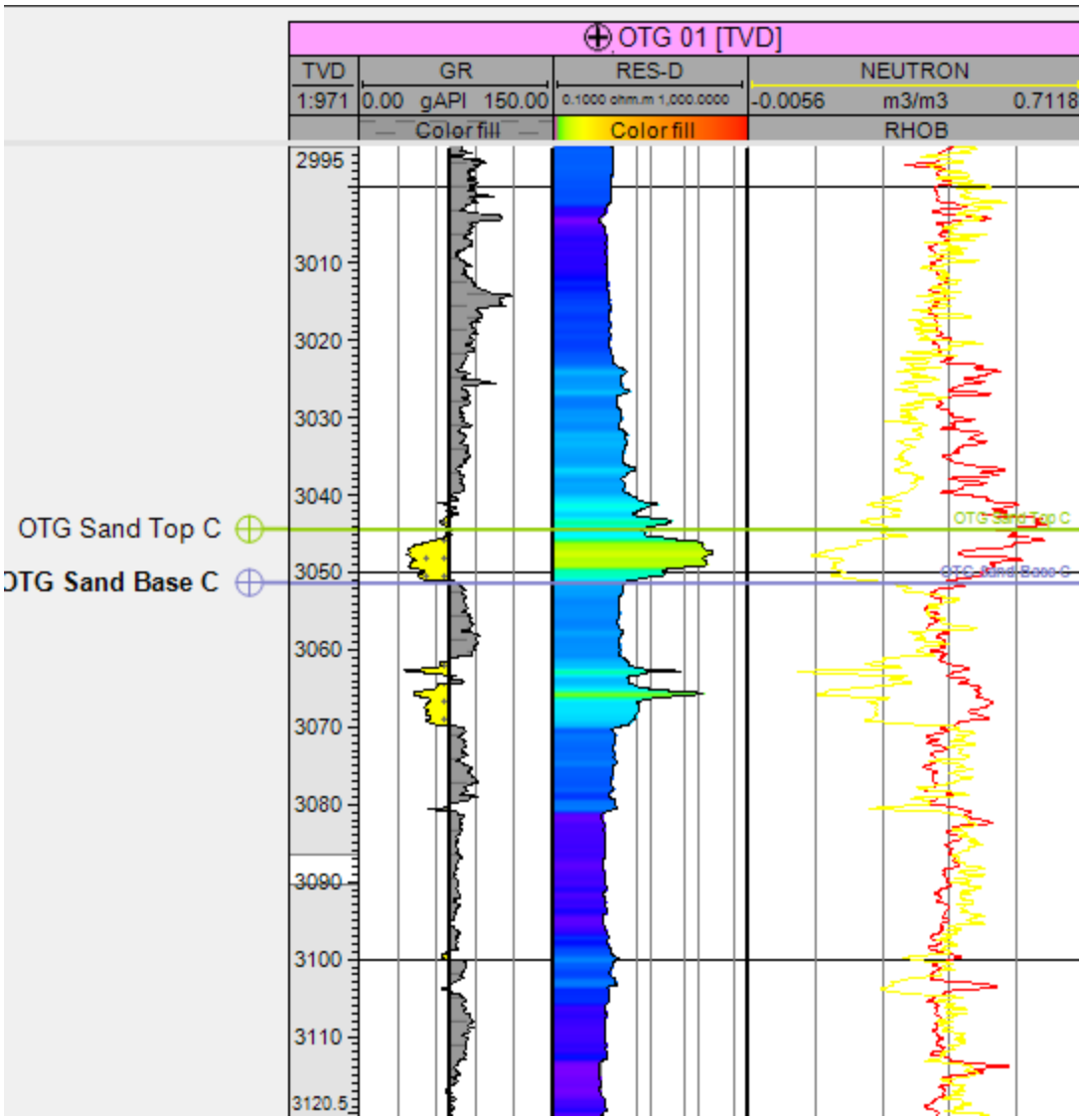

Figure 4.2 Well Section for OTG Sand Top C Reservoir

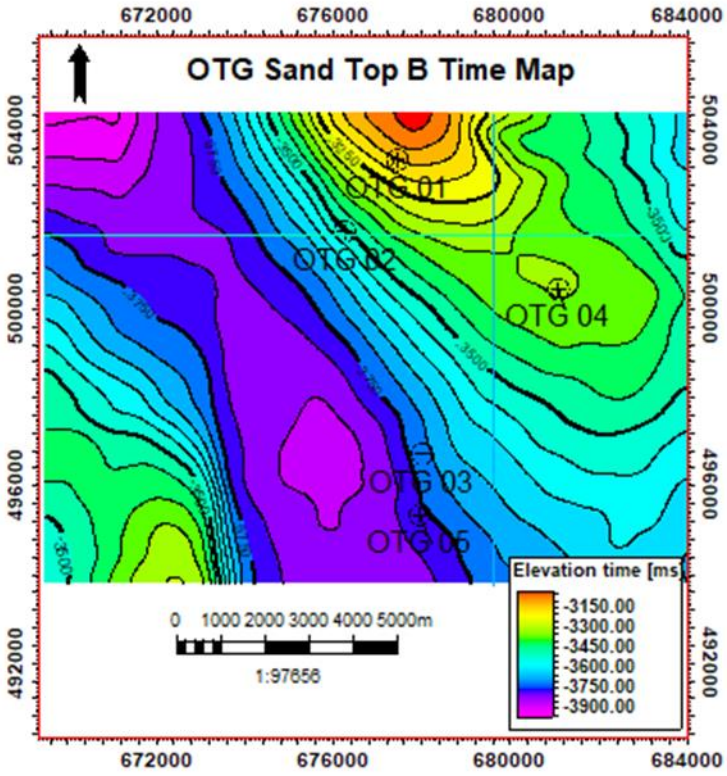

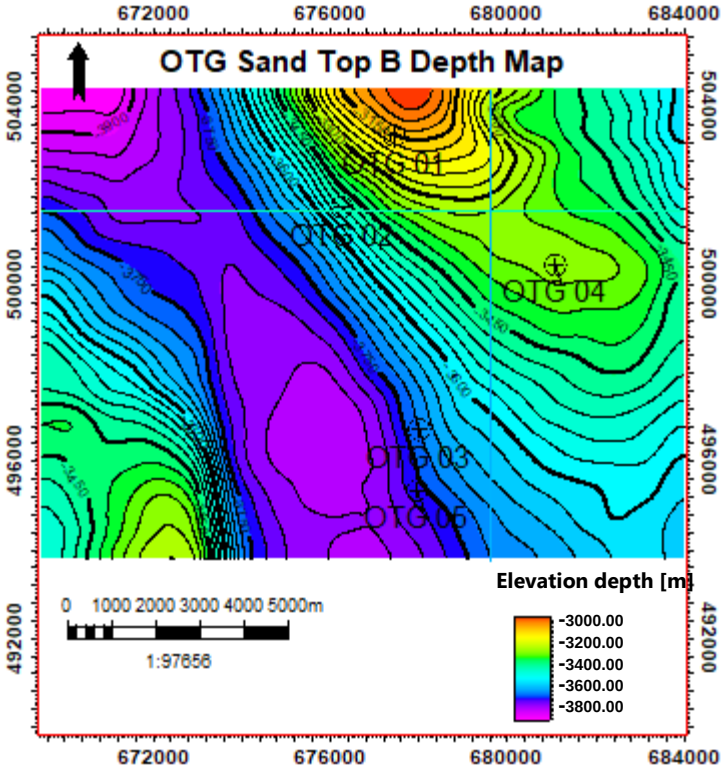

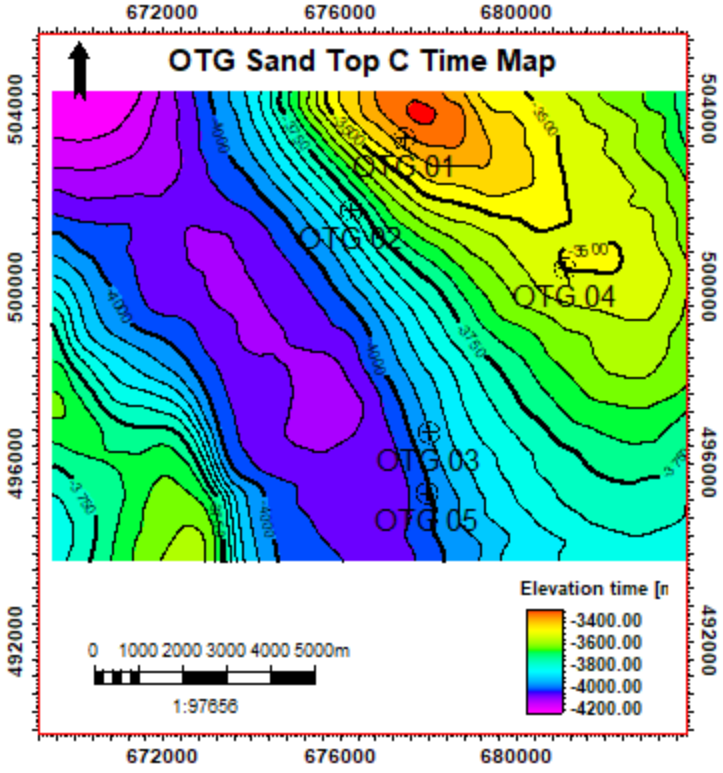

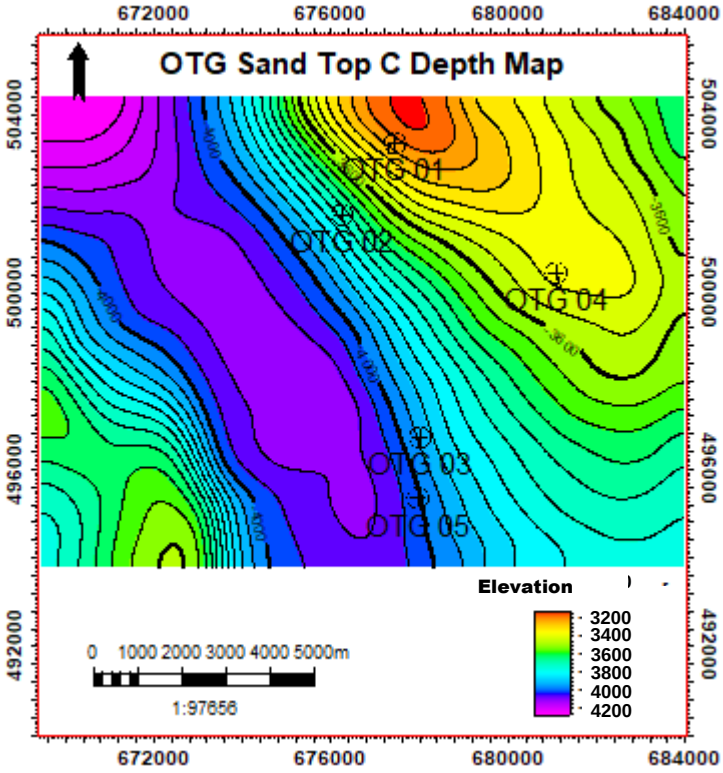

Figure 4.3 (A) OTG Sand Top B Time Map, Figure 4.3 (B) OTG Sand Top B Depth Map

Figure 4.4 (A) OTG Sand Top B Time Map, Figure 4.4 (B) OTG Sand Top B Depth Map

4.1 Attributes Analysis

Seismic attributes analyses carried out on extracted amplitude map for the two reservoir tops (OTG sand top B and OTG SAND Top C) showed that strong amplitude anomalies exist at the OTG 01 well location (Figure 4.4a and 4.4b), OTG 01 well is the case study well. The part of the field where these strong amplitude anomalies were observed corresponded to the location of the OTG 01 well, this further validated the prediction of the occurrence of hydrocarbon within the reservoir in the well. Other parts of the field where the amplitude anomalies were observed also corresponded to the other well locations found in the field particularly for OTG 03 and OTG 04 wells. The seismic amplitude attributes are indicative of hydrocarbon presence.

The root-mean-square (RMS) amplitude attribute was used for the identification of potential hydrocarbon zones because it is more sensitive to direct hydrocarbon indicators (DHIs) and its pattern of bright spot anomaly superposition on the regions of prospectivity are discrete.

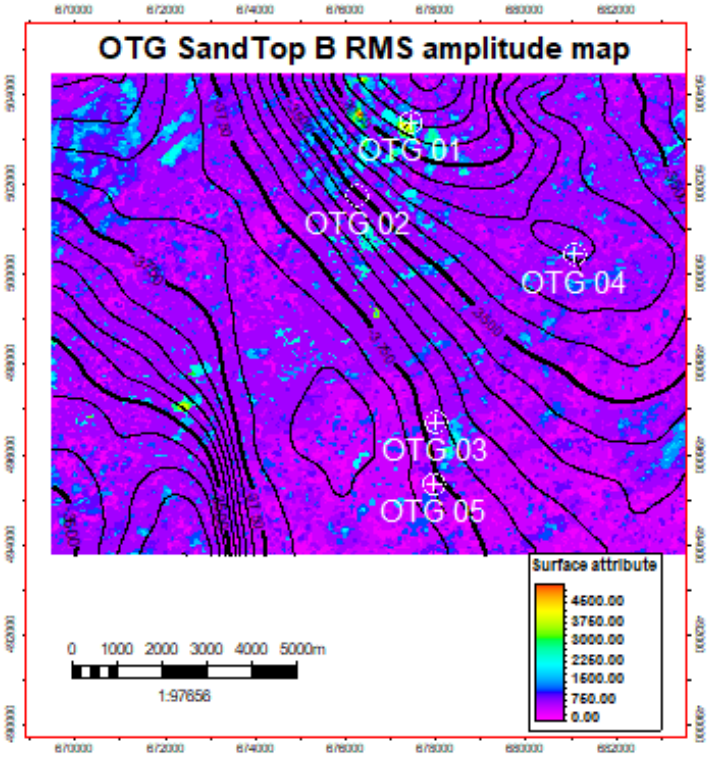

Figure 4.4a OTG Sand Top B RMS Amplitude Map

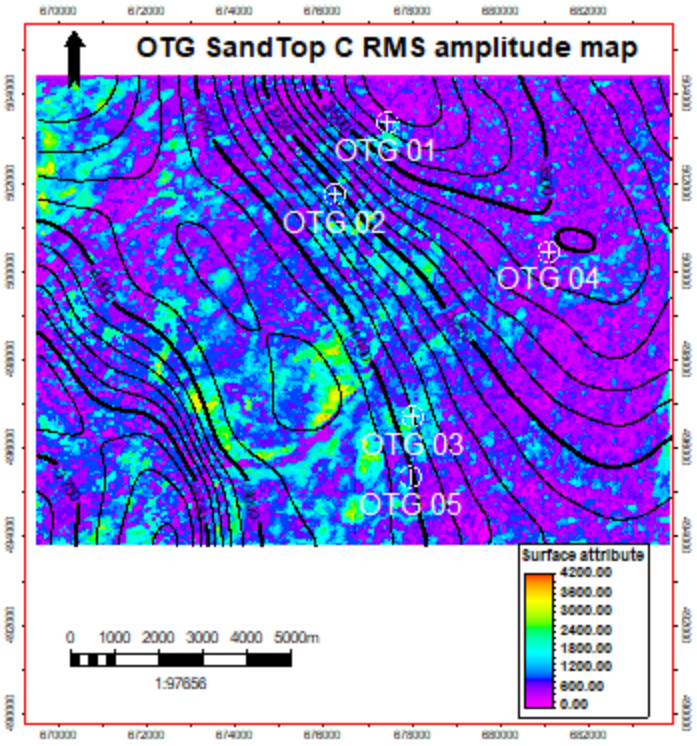

Figure 4.4b OTG Sand Top C RMS Amplitude Map

4.2 Rock Physics Analysis

The nature of the fluid within the reservoir was identified from the physical properties of the reservoir rocks. This is important for better understanding and interpretation of seismic amplitudes in terms of pore fluids and their distribution. Some rock parameters such as velocity of P and S waves, density was plotted against each other. These cross-plots were used to determine the resolution of rock properties in various lithologies in the area, determine the sensitivity of various attributes to fluid effects contribute velocity constraints such as mud rock line values to AVO analysis of seismic data.

Vp/Vs Ratio versus Compressional Travel Time (DTc) Cross plot

It has been established by various studies that Vp/Vs ratio tends to be around 1.58-1.6 for gas it reaches beyond this value in unconsolidated sands and low effective stress regimes (Jain *et al.*

2012). It can be observed that few points fell below the Vp/ Vs value of 1.6 in the cross plot of Vp/Vs ratio versus DTc. This is indicative of gas saturation within the reservoir as shown in the (figure 4.5)

Vp/Vs Ratio vs. Density Cross-plot

This cross-plot of Vp/Vs ratio against density differentiates the region into four zones as illustrated in figure 4.7 The lowest values of the Vp/Vs ratio and density associated with hydrocarbon are validated by low bulk density as observed from the color legend. This plot further confirms the presence of gas within our OTG 01 well. The plot also indicated that the both rock attributes, showed good discrimination.

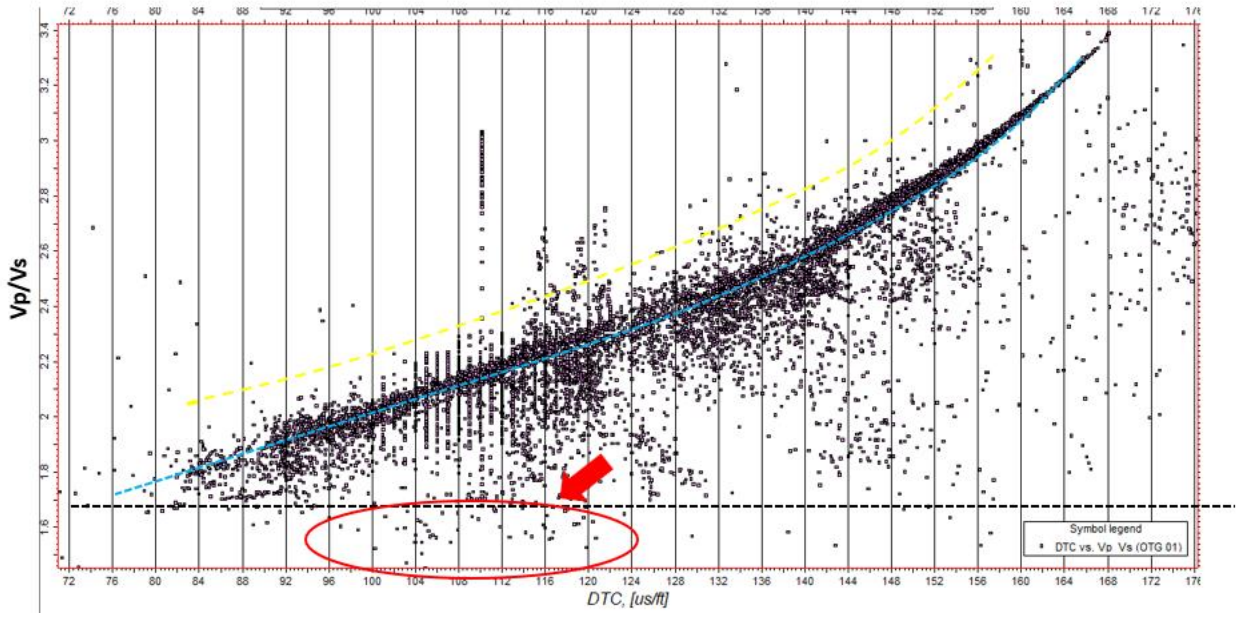

Figure 4.5 Vp/Vs ratio versus dTC Cross-plot

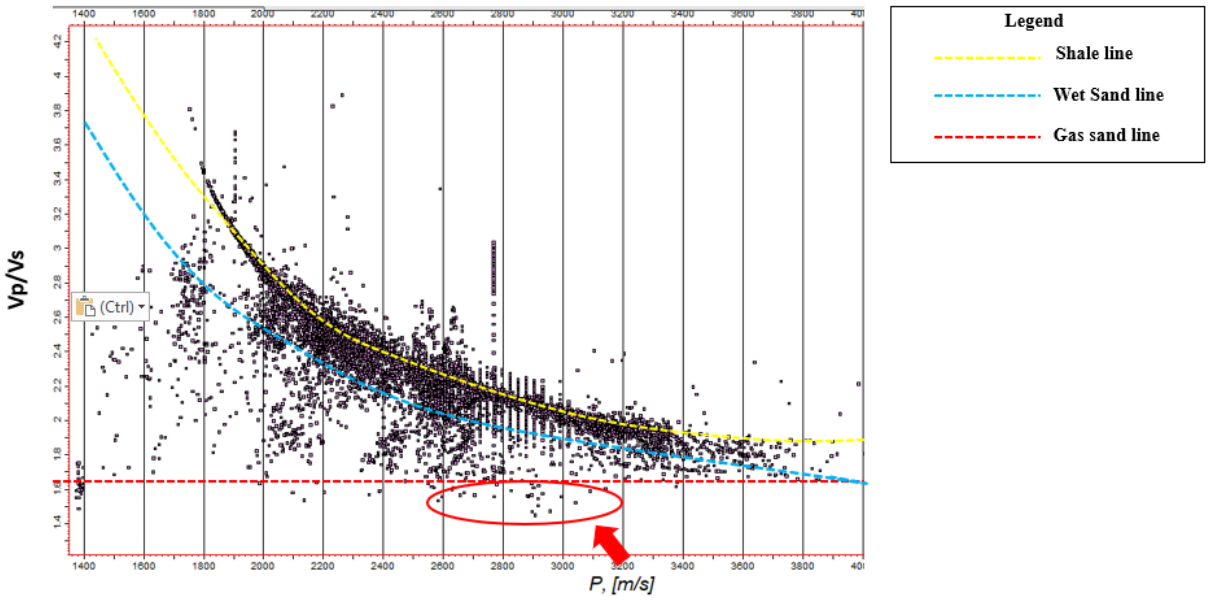

Figure 4.6 Vp/Vs Ratio versus P-wave velocity Cross-plot

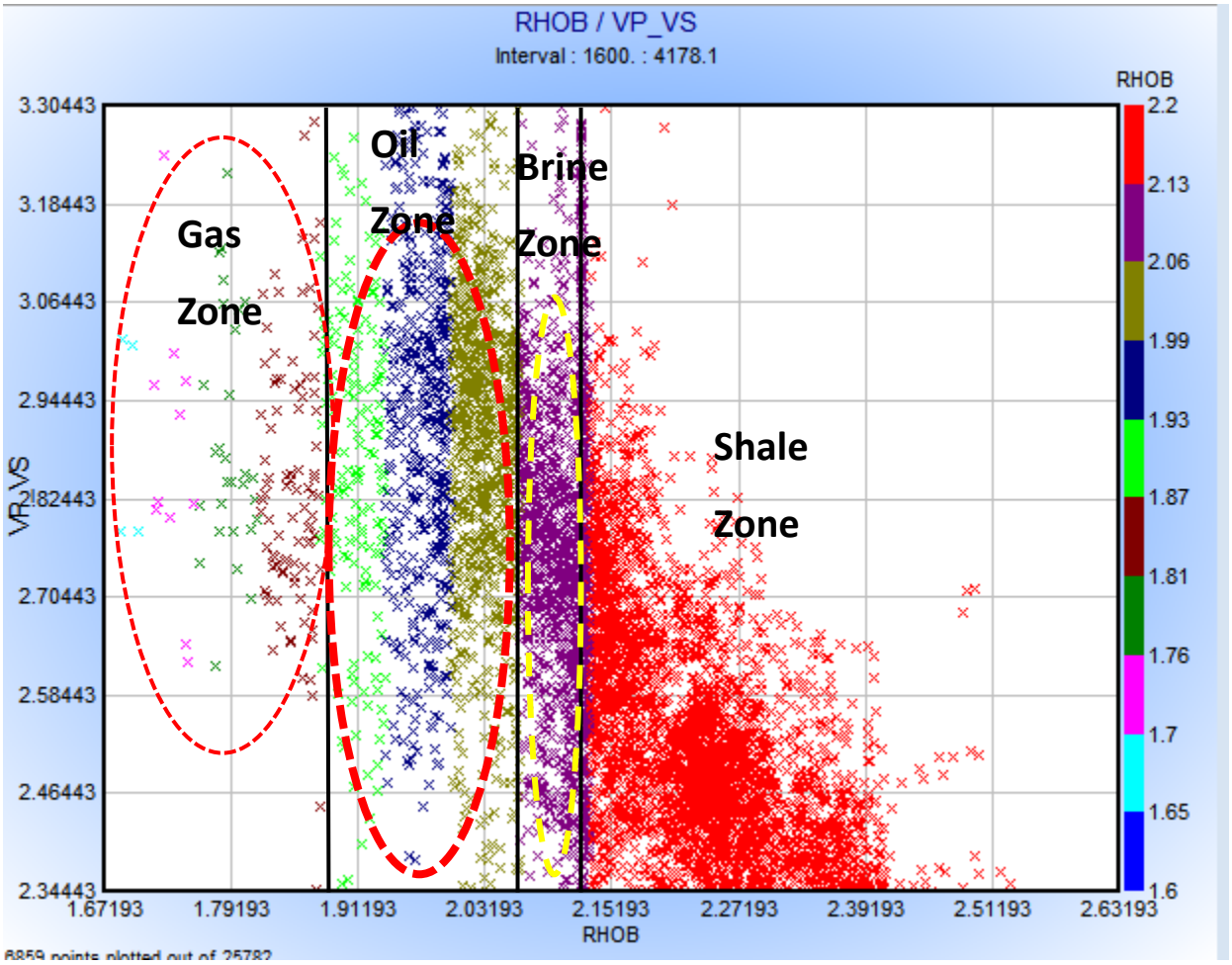

Figure 4.7 Vp/Vs Ratio versus Density Cross-plot

4.3 AVO Analysis

The curves showed a negative gradient, and thus results in a class III AVO anomaly which has higher impedance than the overlying medium, usually shale. A shale-sand interface for these sands has a fairly large positive R_0. The reflection coefficient of a high-impedance sand is positive at zero offset and initially decreases in magnitude with offset. It is indicative of a class III AVO anomaly where the target layer is overlain by a layer of lower impedance values. Class III AVO anomalies have negative reflection and decreased ΔV_s reduces the gradient. The sand is suspected to be poorly compacted and will give off a bright spot on seismic.

4.3.1 Reservoir 1 (Well OTG 01)

The AVO response was then modelled for this reservoir unit at the boundary between the shale and porous sand. Evaluating the gradient curve (figure 4.8), it is observed that the intercept and gradient both decrease as is expected for the addition of hydrocarbons. As the negative amplitude increases, it is expected to brighten in the seismic data. The intercept gradient cross-plot also shows how the data for the brine case lies on the wet trendline and that for the pure oil and pure gas move off this trendline into the top of the lower left hand quadrant denoting a class III low impedance sand, which is expected for the OTG field on the basis of previous works done within the area.

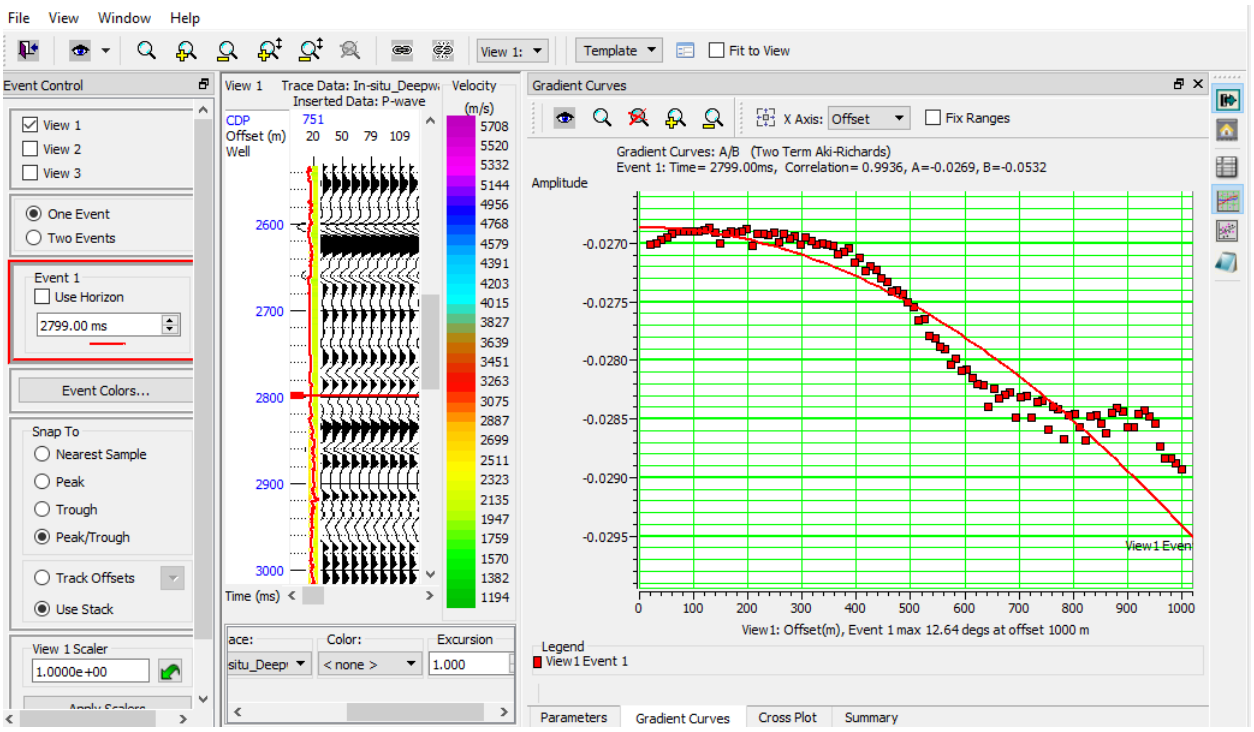

Figure 4.8 Gradient Curve for Reservoir 1

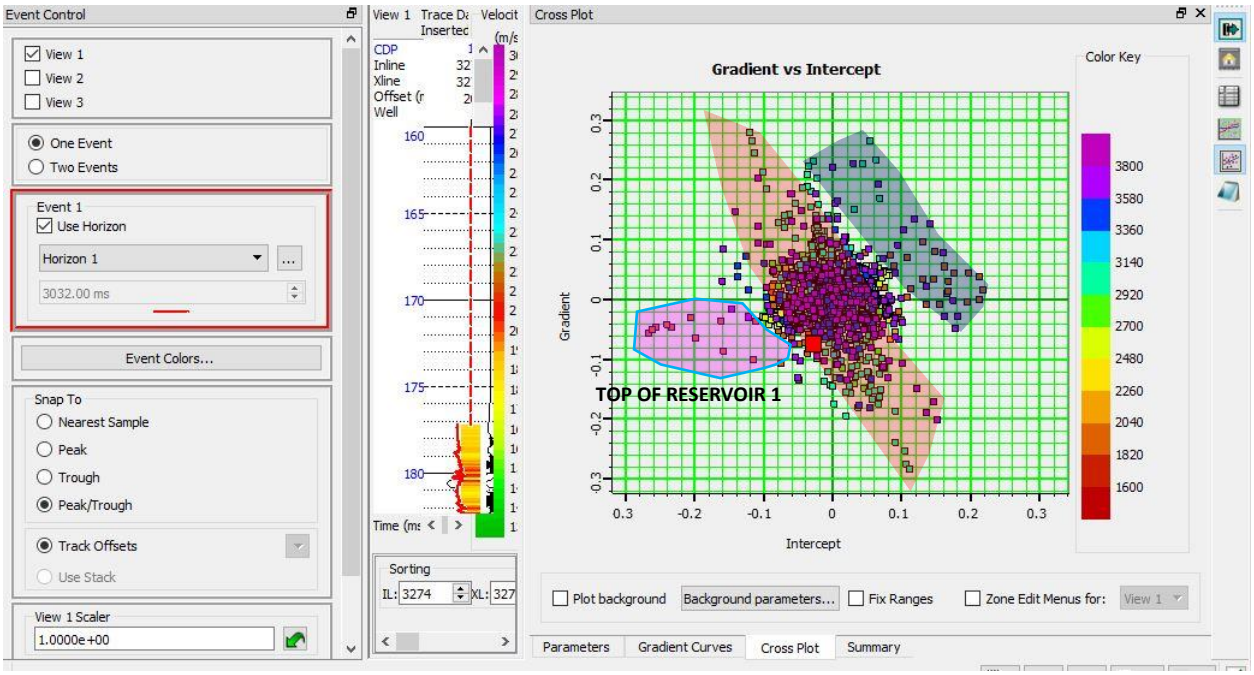

Figure 4.9 Gradient vs Intercept Cross-plot for Reservoir 1

4.3.2 Reservoir 2(Well OTG 01)

The gradient analysis carried out on the real seismic data showed the AVO curves from the analysis having a decrease in amplitude against increasing offset (figure 4.10). By this, the AVO anomaly can be classified as a Class III AVO anomaly according to the Rutherford and Williams (1989) classification of AVO anomalies. It is observed from this class of AVO anomaly that the sands have high porosity, with sediment velocity on the order of 5100 to 8000 ft/sec. This anomaly is due to the presence of light oils and gas, but in this case gas. The same anomaly was observed for both the reservoir tops in this study.

A cross plot of the intercept and gradient data (figure 4.9) showed the anomaly plotting along the fluid line or wet background shale line. This is an indication that the AVO anomaly is hydrocarbon bearing anomaly since the presence of hydrocarbon presents a deviation from the fluid line.

4.3.3 Amplitude Anomaly on Seismic

The amplitudes around the OTG 01 well were carefully observed on the near and far gathers of the seismic data. It was observed that the amplitudes depicted on the far offset gathers (figure 4.12) were more pronounced and larger than the amplitudes in the near offset gathers seismic (figure 4.12. On the other hand, other amplitudes were observed to be unchanged indicated by the blue box, thus confirming that only change(decrease) in amplitude with offset occurred within the region of our reservoir. This observation further corroborates the outcome of the AVO analysis as the gradient curve in both reservoir 1 and 2 indicated a class III anomaly which is represented by decreasing amplitude with increasing offset.

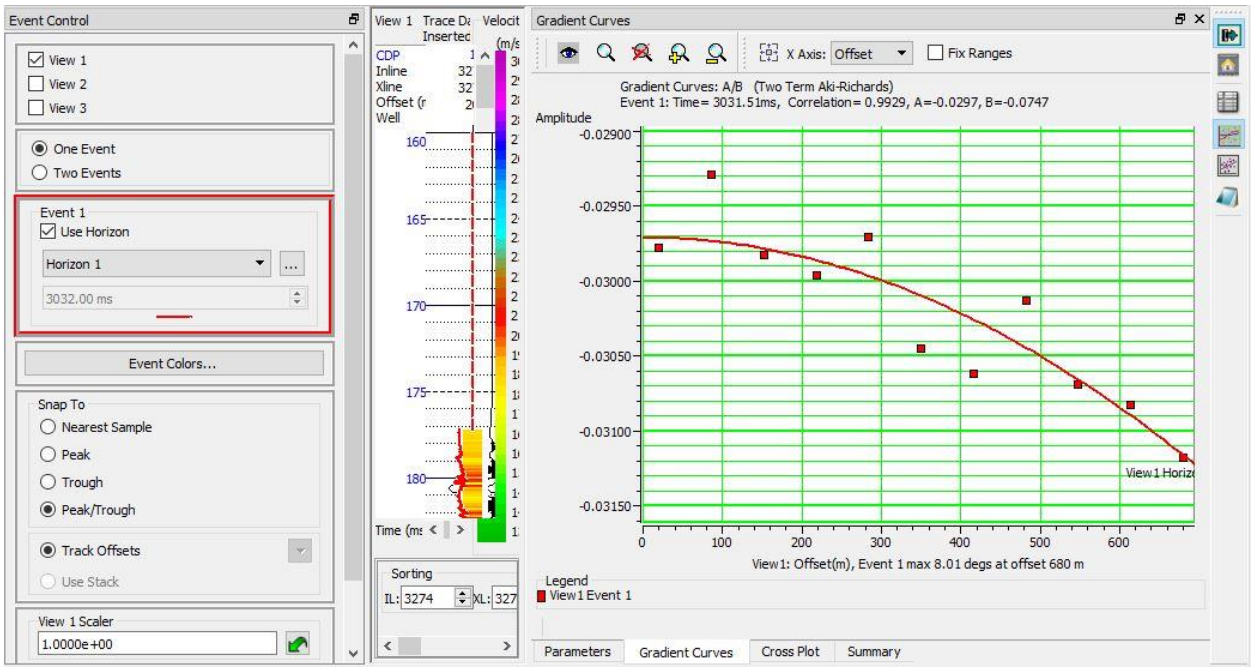

Figure 4.10 Gradient Curve for Reservoir 2

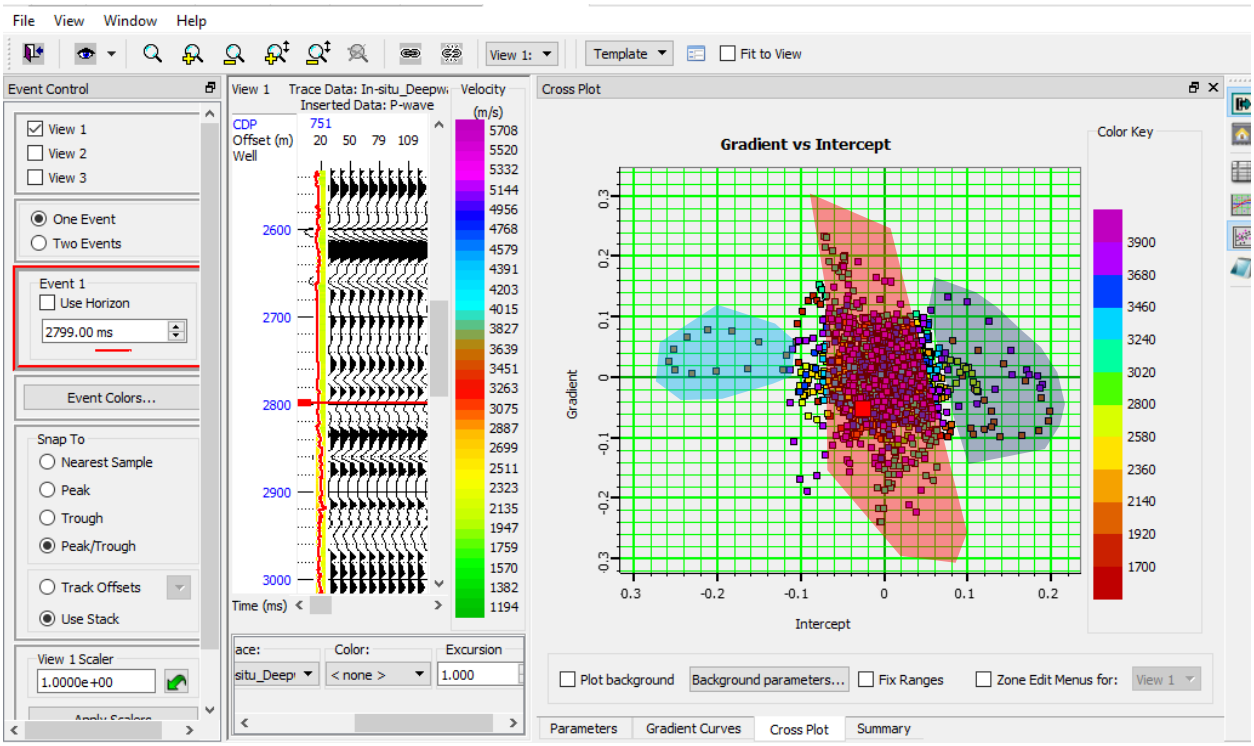

Figure 4.11 Gradient vs Intercept Cross-plot for Reservoir 2

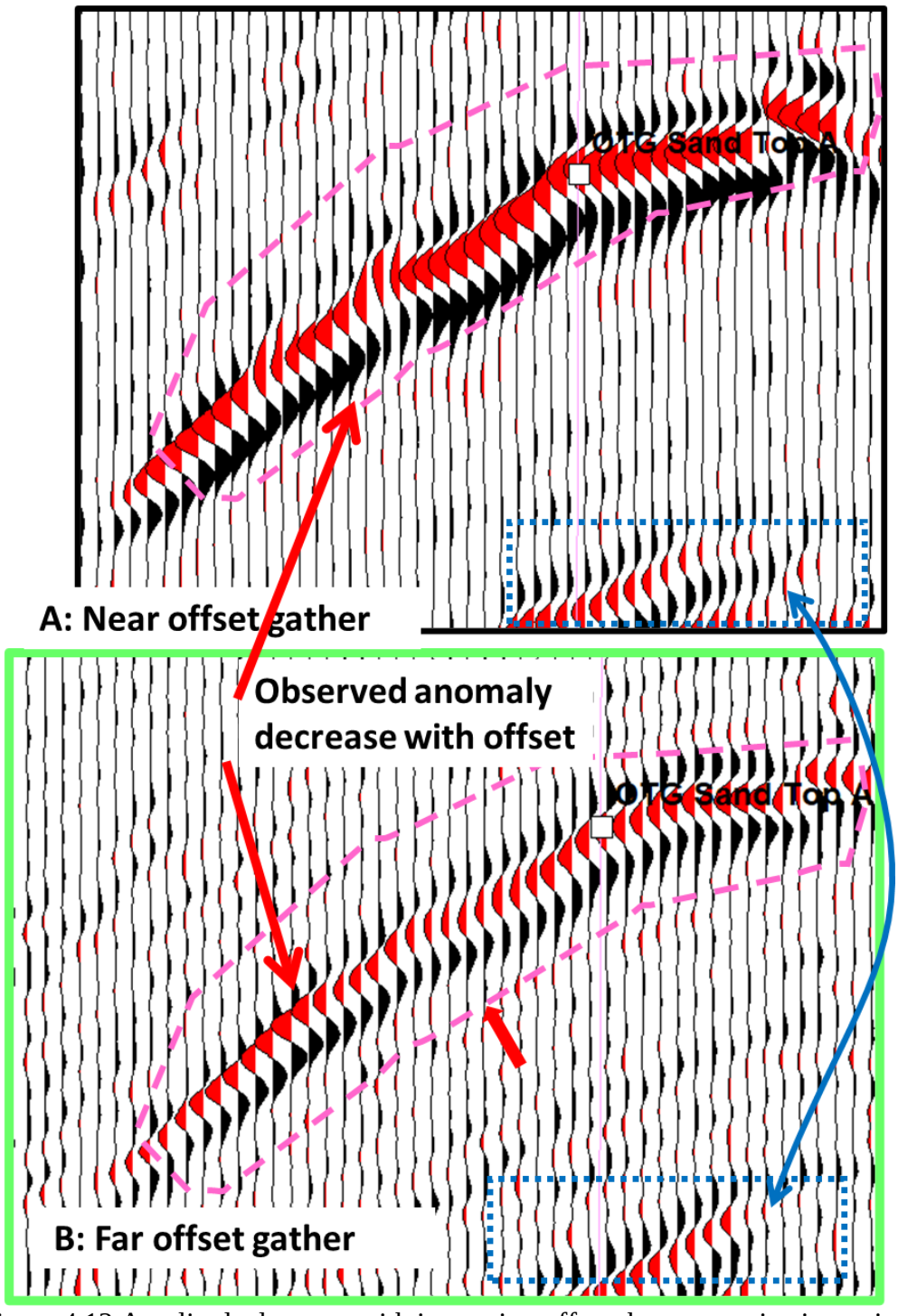

Figure 4.12 Amplitude decrease with increasing offset shown on seismic section.

Chapter Five

5.1 Conclusion

AVO and Seismic attribute analysis has been carried out on OTG field, Deep Offshore, Niger Delta to classify the associated AVO anomaly and ultimately identify the presence of hydrocarbon (gas) in the delineated reservoirs.

Rock attributes such as Vp/Vs ratio against density, Vp/Vs ratio against P-wave velocity and DTc were cross plotted against each other to identify the presence of gas within the reservoirs. The cross plots of Vp/Vs ratio against density and sonic log showed clusters below the gas-sand line on the cross plots and this was interpreted as indicating the presence of gas in the reservoir. The Vp/Vs ratio was also plotted against density and the distribution of fluid within the reservoir were delineated and have shown clusters indicating presence of gas.

Surface attribute analysis carried out using the RMS amplitude which is sensitive to fluid distribution and have shown high amplitude anomaly in regions around the well.

The gradient-intercept cross plots showed clusters deviating from the background trendline and falling into the third quadrant which is expressive of the presence of hydrocarbon (gas).

The AVO anomaly from the evaluation of the gradient curve falls within the classification of class III indicative of gas bearing sands. Therefore, it is expected that the amplitude will decrease with increase in offset. This can be validated by observing the seismic wiggles around the wellbore on the near and far offset gathers. Interestingly, amplitude on the near offset is distinguishably high compared to the far offset.

References

Aki, K. and Richards, P.G. (1980) Quantitative Seismology. Theory and Methods, W.H. Freeman, San Francisco. Vol. 1 and 2.

Allen, J. R. L. (1965). Late Quaternary Niger Delta and Adjacent areas: sedimentary environment and lithofacies. *American Association of Petroleum Geologists*, Vol. 49, 549-600.

Allen, J.L. and Peddy, C.P., (1993). Amplitude Variation with Offset Gulf Coast Case Studies. *Society of Exploration Geophysicists*, Tulsa, OK., 120.

Bancroft, J. C. et al 1997 Pre-stack Seismic Migration & Joint AVO analysis of PP and PS seismic data. *Geophysics*. Vol.83, p. 1-83.

Batzle M, Wang Z (1992) Seismic Properties of Pore Fluids. *Geophysics* Vol. 57, 948–956

Biot, M.A. (1956) Theory of Propagation of Elastic Waves in a Fluid Saturated Porous Solid. II. High Frequency Range. *Journal of the Acoustical Society of America*, Vol. 28, 179-191.

Bortfield. R (1961) Seismic Waves in a Mathematical Model of the Surface Layer, *EAGE Geophysical Prospecting*. Vol. 3, 350-369

Bortfeld, R., (1961) Approximation to the reflection and transmission coefficients of plane longitudinal and transverse waves: *Geophysical Prospecting*., Vol. 9, 485-503.

Box R, Doss E (2008) Typical AVO response as a function of depth and fluid Pressure gradient.

Castagna JP, Swan HW (1997) Principles of AVO Cross Plotting. *Lead Edge* Vol. 16, 337–342

Castagna JP. (1996). AVO Analysis: Tutorial and Review: 1995-1996 SEG Distinguished Lecture condensed from J.P. Castagna and MM. Backus, eds., Offset-Dependent Reflectivity—Theory and Practice of AVO Analysis Society of Exploration Geophysicists, 1993.

J. P. Castagna, M. L. Batzle, and R. L. Eastwood, (1985), "Relationships between compressional- wave and shear- wave velocities in clastic silicate rocks," *Geophysics* Vol. 50: 571-581.

John P. Castagna, De- Hua Han, and Michael L. Batzle, (1995), "Issues in rock physics and implications for DHI interpretation," *The Leading Edge* Vol. 14: 883-886.

Castagna JP (2001) Recent advances in seismic lithologic analysis. *Lead Edge Geophys*. Vol. 66(1)

Chiburis, E.F., 1984, Analysis of amplitude versus offset to detect gas-oil contacts in Arabia Gulf: *54th Ann. Internat. Mtg., Soc. Expl. Geophys., Expanded Abstracts*, 669-670.

Chiburis, E., Franck, C., Leaney, S., McHugo, S., Skidmore, C. 1993. Hydrocarbon Detection with AVO. *Oilfield Review*, Vol. 6, 42– 50.

Craig A. Coulombe et al (1993) Amplitude-versus-offset analysis using the vertical seismic profile.

Dessauvagie, T.F.J. (1972). Stratigraphy of the Embayment near Bida, Nigeria. *African Geology*. p.181 -185.

Doust H, Omatsola E (1990) Niger Delta. In: Edwards JD, Santogrossi PA (eds) Divergent and passive basins. AAPG, Tulsa

Duffat K, Landro M (2007) Spectral VP/Vs ratio versus differential stress and rock consolidation—a comparison between rock models and time-lapse AVO data. Geophysics 72(5):C81–C94

Ebong D. Ebong et al 2018. Stochastic modelling of spatial variability of petrophysical properties in parts of the Niger Delta Basin, southern Nigeria.

Evamy, et al. (1978). Hydrocarbon Habitat of the Tertiary Niger Delta. *American Association of Petroleum Geologists Bulletin*. Vol.62. p. 1-39

Foster DJ, Robert GK, Lane FD (2010) Interpretation of AVO Anomalies. Geophysics

Ogochukwu F. O and Edmund. (2014*) A Adv. Appl. Sci. Res*., Vol. 5(5):148-164

Gardner GHF, Gardner LW, Gregory AR (1974) Formation Velocity and Density- The Diagnostic Basics for Stratigraphic Traps. *Geophysics* Vol.39: 770-780.

Gassmann F (1951) Elastic waves through a packing of spheres. *Geophysics* 16:673–685

Gelfand, V., et al, 1986: "Seismic Lithologic Modeling of Amplitude-versus-offset Data", *Proceedings of the 56th Annual Meeting of the SEG*, Nov. 2-6, 1986, p. 334-336

Goodway, B., Chen, T., Downton, J. 1997. Improved AVO fluid detection and lithology discrimination using Lame's petrophysical parameters. Expanded Abstracts. CSEG, 1997 Convention

Goodway et al. (1998) AVO analysis to extract rock parameters on the Blackfoot 3C-3D seismic data. *SEG Expanded Abstracts* 1998.

Hanafy, S., Nimmagadda, S.L., Mahmoud, S.E. *et al.* Regional integrated interpretation of the hydrocarbon prospectivity of the Nile Delta, Offshore Egypt. *Arab J Geosci* **9,** 376 (2016).

Henry Ohaegbuchu, Magnus Igboekwe (2016) Determination of Subsurface rock properties from AVO analysis in Konga oil field of the Niger Delta, Southeastern Nigeria. Model. *Earth Syst. Environ*. (2016) 2:124

Knott, C.G., (1899) Reflexion and Refraction of Elastic Waves with Seismological Applications*: Phil. Mag*., Vol. 48, 64-97.

Koefoed O (1955) On the effect of Poisson's ratios of rock strata on the reflection coefficients of Plane Waves. *Geophysical Prospecting* 3: 381-387.

Koefoed O (1962) Reflection and Transmission Coefficients for Plane Longitudinal Incident Waves. *Geophys Prospect* Vol. 10:304–351

Professor C. G. Knott D.Sc. F.R.S.E. (1899) III. *Reflexion and refraction of elastic waves, with seismological applications,* The London, Edinburgh, and Dublin Philosophical Magazine and Journal of Science, 48:290, 64-97

Kulke H (1995) Regional Petroleum Geology of the World. Part II: Africa, America, Australia and Antarctica*: Berlin, Gebruder Borntraeger,* p. 143-172.

Kukumon Adeoti. et.al (2015) Fluid prediction using AVO analysis and forward modelling of deep reservoirs in Faith Field, Niger Delta, Nigeria Arab J Geosci (2015) 8:4057–4074

Mitchel Xavier (Halliburton) and Rodrigo S. Portugal (Halliburton) AVO Analysis in Real Pre-Stack Seismic Data: A Powerful Tool for Fluid Identification During Petroleum Exploration

Ostrander, W. J., (1982) Plane wave reflection coefficients for gas sands at non-normal angles of incidence: Presented at the 52nd Annual SEG Meeting, Dallas

Reyment, R. A. (1965). Aspects of the geology of Nigeria. The Stratigraphy of the Cretaceous and Cenozoic deposits. *Ibadan University Press*. 23-73.

Russell BH, Hedlin K, Hilterman FJ, Lines LR (2001) Fluid-property discrimination with AVO: a Biot-Gassmann perspective. *CREWES Res Rep 13(1)*:403–419

Rutherford SR, Williams RH (1989) Amplitude-versus-offset variations in gas sands. Geophysics 54:680–688

Swan HW (2001) Velocities from amplitude variations with offset. *Geophysics* 66(6):1735–1743

Short, K.C. and Stauble, A. 1967. Outline Geology of Niger Delta, American Association of Petroleum Geologists.

Shuey RT (1985) A simplification of the Zoeppritz equations. *Geophysics* Vol. 50 p. 609-614.

Smith GC, Gidlow PM (1987) Weighted Stacking for Rock Property Estimation and Detection of Gas. *Geophysical Prospecting.* Vol. 35 p. 993-1014.

Stacher, P. (1995). Present Understanding of the Niger Delta hydrocarbon habitat, In, M. N Oti and G. Postma (eds.), *Geology of Deltas*: Rotterdam, A.A. Balkema, p. 257-267.

Uko ED, Emudianughe JE (2014) AVO Modelling of the South-East Niger Delta, Nigeria. J *Geophys Remote Sensing* Vol.3 p. 131

Verm and Hilterman (1995) Lithology color-coded seismic sections; The Calibration of AVO Cross Plotting to Rock properties.

Whiteman A (1982) Nigeria: Its Petroleum Geology, Resources and Potential: *London, Graham and Trotman,* p. 394.

Xiao, H. and Suppe, J. (1992). Origin of Rollover. *American Association of Petroleum Geologists Bulletin,* Vol. 76, pp. 509-229.

Yilmaz ÖZ (2001) Seismic data analysis: processing, inversion, and interpretation of seismic data. *Soc Explor Geophys Tulsa II*:2024

Zhang, H., and Brown, R. J., (2001), A review of AVO analysis: *CREWES Research Report*, Vol. 13.

Zoeppritz K (1919). Earthquake waves VIII B, About reflection on the passage of seismic waves through discontinuity surfaces: *Göttinger Nach* Vol. 2 366-84.